

This is an Open Access document downloaded from ORCA, Cardiff University's institutional repository: <https://orca.cardiff.ac.uk/id/eprint/112105/>

This is the author's version of a work that was submitted to / accepted for publication.

Citation for final published version:

Pucilowska, Joanna, Vithayathil, Joseph, Pagani, Marco, Kelly, Caitlin, Karlo, J. Colleen, Robol, Camila, Morella, Ilaria, Gozzi, Alessandro, Brambilla, Riccardo and Landreth, Gary E. 2018. Pharmacological inhibition of ERK signaling rescues pathophysiology and behavioral phenotype associated with 16p11.2 chromosomal deletion in mice. *Journal of Neuroscience* 38 (30), pp. 6640-6652.
10.1523/JNEUROSCI.0515-17.2018

Publishers page: <http://dx.doi.org/10.1523/JNEUROSCI.0515-17.2018>

Please note:

Changes made as a result of publishing processes such as copy-editing, formatting and page numbers may not be reflected in this version. For the definitive version of this publication, please refer to the published source. You are advised to consult the publisher's version if you wish to cite this paper.

This version is being made available in accordance with publisher policies. See <http://orca.cf.ac.uk/policies.html> for usage policies. Copyright and moral rights for publications made available in ORCA are retained by the copyright holders.



1 **Title:**

2

3 **Pharmacological Inhibition of ERK Signaling Rescues Pathophysiology and Behavioral**
4 **Phenotype Associated with 16p11.2 Chromosomal Deletion in Mice.**

5

6 **Abbreviated title:**

7 **Novel ERK inhibitor rescues deficits in a mouse model of autism.**

8 **Authors:**

9 J. Pucilowska¹, J. Vithayathil¹, M. Pagani², C. Kelly¹, J. C. Karlo¹, C. Robol², I. Morella³, A.
10 Gozzi², R. Brambilla³, and G.E. Landreth^{1,4}

11 ¹Department of Neurosciences, Case Western Reserve University, Cleveland, Ohio 44106-4928

12

13 ² Functional Neuroimaging Laboratory, Istituto Italiano di Tecnologia, Center for Neuroscience
14 and Cognitive Systems @ UNITN Corso Bettini 31, 38068 Rovereto, Italy

15

16 ³ Neuroscience and Mental Health Research Institute and School of Biosciences, Cardiff
17 University, Cardiff, UK. ^{[[[}
_{SEP]}

18 ⁴ Stark Neuroscience Research Institute, Indiana University School of Medicine, Indianapolis, IN
19 46202

20

21

22

23 **Corresponding Author:**

24 Dr. Gary Landreth
25 Stark Neuroscience Research Institute
26 Indiana University School of Medicine
27 320 W. 15th St., NB214C
28 Indianapolis, IN 46202
29 317 278 7820- office
30 Email: glandret@iu.edu
31

32

33 **Number of pages:** 38

34

35 **Number of figures:** 7

36

37 **Number of words:** Abstract (143), Significance Statement (120), Introduction (585),

38 Discussion(1484)

39

40

41 **Conflict of Interest:** The authors declare no competing financial interests.

42

43

44

45

46 **Acknowledgements:** This work was supported by grants from the Simons Foundation
47 (SFARI 275316, GEL). A. Gozzi acknowledges funding from the Simon Foundation (SFARI
48 314688 and 400101, AG) and the Brain and Behavior Foundation (NARSAD, AG). I. Morella
49 acknowledges support from the Waterloo Foundation.

50

51

52

53

54 **Abstract:**

55 The human *16p11.2* microdeletion is one of the most common gene copy number variations
56 linked to autism, but the pathophysiology associated with this chromosomal abnormality is
57 largely unknown. The 593-kb deletion contains the ERK1 gene and other genes that converge
58 onto the ERK/MAP kinase pathway. Perturbations in ERK signaling are linked to a group of
59 related neurodevelopmental disorders hallmarked by intellectual disability, including autism. We
60 report that mice harboring the *16p11.2* deletion exhibit a paradoxical elevation of ERK activity,
61 cortical cytoarchitecture abnormalities and behavioral deficits. Importantly, we show that
62 treatment with a novel ERK pathway inhibitor during a critical period of brain development
63 rescues the molecular, anatomical and behavioral deficits in the *16p11.2* deletion mice. The ERK
64 inhibitor treatment administered to adult mice ameliorates a subset of these behavioral deficits.
65 Our findings provide evidence for potential targeted therapeutic intervention in *16p11.2* deletion
66 carriers.

67 **Significance Statement:**

68 The ERK/MAPK pathway is genetically linked to autism spectrum disorders and other
69 syndromes typified by intellectual disability. We provide direct evidence connecting the ERK/
70 MAP kinases to the developmental abnormalities in neurogenesis and cortical cytoarchitecture
71 associated with the *16p11.2* chromosomal deletion. Most importantly, we demonstrate that
72 treatment with a novel ERK specific inhibitor during development rescues aberrant cortical
73 cytoarchitecture and restores normal levels of cell cycle regulators during cortical neurogenesis.
74 These treatments partially reverse the behavioral deficits observed in the *16p11.2del* mouse
75 model, including hyperactivity, memory as well as olfaction, and maternal behavior. We also
76 report a rescue of a subset of these deficits upon treatment of adult *16p11.2del* mice. These data

77 provide a strong rationale for therapeutic approaches to this disorder.

78 **Introduction:**

79 Autism Spectrum Disorders (ASDs) are complex, highly heritable neurodevelopmental
80 disorders affecting approximately 1 in 100 children. Copy number variations (CNVs) and other
81 chromosomal rearrangements are associated with approximately 10-20% of ASDs. CNV of
82 human chromosome *16p11.2* is one of the most common genetic linkages to autism and deletion
83 of this region accounts for approximately 1% of ASDs (Levy et al., 2011). Individuals
84 heterozygous for the *16p11.2* deletion exhibit a range of clinical symptoms including ASD,
85 language impairment, intellectual disability (ID), anxiety, attention deficit hyperactivity disorder
86 and epilepsy (Ghebranious et al., 2007; Zufferey et al., 2012; Hanson et al., 2015a). The human
87 *16p11.2* locus contains 27 genes, which includes the *MAPK3* gene (encoding ERK1) and the
88 Major Vault Protein gene (*MVP*), both of which converge onto the ERK/MAP kinase pathway
89 (Kumar et al., 2007).

90 The extracellular signal-regulated kinases, ERK1 and ERK2, are central elements of one
91 of the most prominent intracellular signaling cascades, the Mitogen Activated Protein Kinase
92 (MAPK) pathway. The ERKs play critical roles in brain development and synaptic plasticity
93 (Sweatt, 2004) and are activated in response to a broad range of stimuli including growth factors,
94 neurotransmitters, morphogens and transient increases in synaptic Ca²⁺ (Roskoski, 2012).
95 Importantly, they are genetically linked to ASDs and other syndromes typified by ID (Marshall
96 et al., 2008; Wen et al., 2016; Borrie et al., 2017; Mitra et al., 2017). Mutations in elements of
97 the ERK/MAPK pathway alter the activity of the ERKs, resulting in a group of genetic disorders
98 collectively known as “RASopathies”. These syndromes are typified by ID, developmental and
99 language deficits, ASD and psychiatric disease (Tidyman and Rauen, 2009; Fasano and

100 Brambilla, 2011).

101 We have previously reported that a murine model of the *16p11.2* human microdeletion
102 (*16p11.2del*) exhibits a reduction in brain size and perturbations in cortical
103 cytoarchitecture, which are postulated to be due to impaired ERK-mediated regulation of neural
104 progenitor proliferation (Newbern et al., 2008; Pucilowska et al., 2015). The *16p11.2del* mice
105 exhibit a paradoxical increase in ERK signaling coincident with aberrant cortical neurogenesis,
106 ultimately resulting in behavioral deficits analogous to the *16p11.2* microdeletion carriers
107 (Portmann et al., 2014; Hanson et al., 2015b). Therefore, we postulated that treatment with brain
108 permeable Ras-ERK pathway inhibitors may correct the pathophysiology associated with the
109 *16p11.2* deletion. Recently, we have validated two novel cell permeable peptides (CPPs), RB1
110 and RB3, that efficiently inhibit Ras-ERK signaling in the post-natal developing brain and rescue
111 morphological impairments in a severe mouse model of RASopathies (Papale et al., 2017). In
112 addition, the RB1 and RB3 peptides are able to block cocaine-mediated ERK activation and the
113 associated behavioral response (Papale et al., 2016).

114 In this study, we report that prenatal treatment with cell permeant RB1/RB3 peptides
115 rescues developmental deficits in neurogenesis in the embryo and subsequently restores normal
116 neuronal numbers and cortical cytoarchitecture in the *16p11.2del* mice. Specifically, we report
117 restoration of hippocampal based memory function, anxiety, olfaction, maternal behavior as well
118 as hyperactivity in the *16p11.2del* mice. Furthermore, postnatal drug treatment of adult
119 *16p11.2del* mice results in partial amelioration of the behavioral deficits, suggesting a broader
120 window for pharmacologic intervention. To assess the macroscale anatomical substrates affected
121 by the drug treatment, we used high-resolution morphoanatomical MRI mapping to show partial
122 restoration of gray matter volume in ventral hippocampal and lateral septal regions, which we

123 found to be reduced in the *16p11.2del* mice. We conclude that treatment with ERK pathway
124 inhibitors may represent a potential therapeutic intervention in *16p11.2del* carriers, as has been
125 suggested for RASopathies (Tidyman and Rauen, 2009). This is the first example of the rescue
126 of development abnormalities in this ASD model.

127

128 **Materials and Methods:**

129 **Animals.** A mouse line carrying a microdeletion on chromosome *7qF3*, the syntenic region of
130 human chromosome *16p11.2*, was generated by A. Mills and purchased from Jackson Labs
131 (Horev et al., 2011). This mouse line has been maintained on a fixed ratio, mixed (129/C57)
132 background with large numbers of mice examined to minimize any genetic background-
133 associated variation. Embryonic and adult treatments were 5 days long and administered by sub-
134 cutaneous injections of ERK inhibitor resuspended in PBS at a dose of 10mg/kg. Pregnant dams
135 were used with a plug date designated as 0.5 days.

136

137 **Drugs:** RB1 and RB3 cell permeable peptides have been recently described (Papale et al., 2016).
138 Briefly, RB1 was designed around residues 59-73 within the KIM sequence of the ERK-specific
139 phosphatase MKP3 (Liu et al., 2006) that interacts with a docking motif required for interactions
140 of ERK1/2 with both its regulators and substrates. RB3 was designed, using the MOE software
141 package, (Molecular Operating Environment, version 10.10, Chemical Computing group,
142 Montreal Canada, <http://www.chemcomp.com>) by aligning and superposing the CDC25 domain
143 of Ras-GRF1 (Freedman et al., 2006) the published crystal structure of a ternary
144 Ras:SOS:Ras*GDP complex (Sondermann et al., 2004) using the default settings. The
145 interacting surface between the two proteins was then visually analyzed and the portion of the

146 CDC25 domain between residues 1173 to 1203 was selected for the preparation of the final
147 peptide. RB1 (MGRKKRRQRRRPPQAPGIMLRRLQKGNLPVSRYPYDVPD), SCR RB1
148 (MGRKKRRQRRRPPQALSCLKRLRSRGMNRTSATQSRYPYD), RB3
149 (GRKKRRQRRRPPCVPYLGMYLTDLVFIEEGTPNYTEDGLVN) and SCR RB3
150 (GRKKRRQRRRPPCFEVYPDSGDYTYEGELNGTLMVVPTN) were custom synthesized by
151 GENECAST EUROPE (Luxembourg).

152 For *in vivo* experiments, batches of 200 mg, highly purified by high-performance liquid
153 chromatography (HPLC) ($\geq 95\%$) with C-terminal amino acid (last) in D form and acetylated N-
154 Terminal (first) amino acid were used. The peptides were dissolved in PBS 1X and injected 10
155 mg/kg (i.p.) (10 mg/kg each peptide) intraperitoneally.

156 **Sample preparation and MRI acquisition:** High-resolution morpho-anatomical T2-weighted
157 MR imaging of P90 *ex vivo* mouse brains was performed in paraformaldehyde fixed specimens.
158 Standard sample preparation and MRI acquisition have been recently described in detail (Cutuli
159 et al., 2016). Briefly, *16p11.2del* mice and age-matched control littermates (treated with ERK
160 inhibitor or vehicles) were deeply anesthetized and their brains were perfused *in situ* via cardiac
161 perfusion. The perfusion was performed with phosphate buffered saline followed by
162 paraformaldehyde (4% PFA; 100 ml). Both perfusion solutions included a gadolinium chelate
163 (Prohance, Bracco, Milan) at a concentration of 10 and 5 mM, respectively, to shorten
164 longitudinal relaxation times. Brains were imaged inside intact skulls to avoid post-extraction
165 deformations. A multi-channel 7.0 Tesla MRI scanner (Bruker Biospin, Milan) was used to
166 acquire anatomical images of the brain, using a 72 mm birdcage transmit coil and a custom-built
167 saddle-shaped solenoid coil for signal reception, with the following imaging parameters: FLASH

168 3D sequence with TR = 17 ms, TE = 10 ms, alpha = 30°, matrix size of 260 × 180 × 180, field of
169 view of 1.82 × 1.26 × 1.26 cm and voxel size of 0.07 mm (isotropic).

170 **Tensor Based Morphometry (TBM) automated anatomical labeling and structural**
171 **covariance MRI network mapping.** Inter-group morpho-anatomical differences in local
172 volumes were mapped with TBM (Ashburner & Friston, 2000) using ANTs (Avants et al., 2009).
173 The registration-based TBM procedure employed has been thoroughly described elsewhere
174 (Pagani et al., 2016). First, all the high-resolution T2-weighted images were corrected for
175 intensity non-uniformity and skull stripped to remove extra-brain tissue. A study-based template
176 was then created aligning pre-processed images to a common reference space using affine and
177 diffeomorphic registrations. Individual images of *16p11.2del* and control mice (treated with ERK
178 inhibitor or vehicle) were registered to the study-based template and the Jacobian determinants
179 of the deformation fields were calculated at each voxel, giving the voxel's relative expansion or
180 contraction in the space of the study-based template. Jacobian determinants were also normalized
181 by the total intracranial volume to further eliminate overall brain volume variations. We
182 measured non-normalized intracranial brain volume in all the four treatment groups at P90 . The
183 results we obtained showed the presence of smaller brain volume in 16p11.2 mutants, a finding
184 previously reported in mice modelling 16p11.2 deletion (Portmann et al., 2014). The treatment
185 did not affect total intracranial volume in either WT or *16p11.2* mutants. The resulting maps
186 were smoothed using a Gaussian kernel with a sigma of three voxel width and employed for
187 voxel-wise statistics. Regional volume differences between *16p11.2del* and control mice were
188 mapped by fitting a GLM ($t > 2.3$) followed by a cluster correction using a significant cluster
189 threshold of $p = 0.01$ (Worsley et al., 1992) as implemented in FSL. We also employed
190 preprocessed images to independently calculate volumes of brain regions via automated

191 anatomical labeling (Pagani et al., 2016), using two neuroanatomically parcellated reference
192 MRI atlases for cortical (Ullmann et al., 2013) and subcortical areas (Dorr et al., 2008).

193 **Behavioral analysis.** Three-month-old male and female mice were utilized for standardized
194 behavioral analyses including the elevated plus maze, open-field, novel object recognition,
195 olfaction, maternal behavior and **fear conditioning tests** in **order as stated**. All tests were
196 conducted in a designated behavior room during the light cycle between 9:00 A.M. and 6:00
197 P.M. A maximum of 5 mice of mixed genotypes were housed together with ad libitum access to
198 food and water with a 12 h light/dark cycle. All equipment was cleaned with 70% ethanol after
199 each use to remove odor cues. The tester was blinded to the genotype of each animal. All tests
200 were performed at the Case Western Reserve University Rodent Behavior Core. Three different
201 cohorts (each with at least 50 mice divided to include both genotypes and treatment paradigms)
202 were evaluated in three independent experiments. The data represents the pooled analysis of all
203 three cohorts.

204 The elevated plus maze: The maze consisted of two open and two closed arms crossing each
205 other approximately 1 m above the floor. The maze was fitted with infrared grid and video
206 tracking system (Med Associates Inc.). Individual test mice were placed in the center facing the
207 open arm and their activity was recorded for 5 minutes. The % time spent in open and closed
208 arms, the number of entries into each arm, number of head dips and frequency of
209 urination/defecation were scored.

210 Open field test: A box (40cm x 40cm) was placed in a dimly lit environment. EthoVision XT 5.0
211 (Noldus) was used to digitally subdivide the box area into a 20 cm Å~ 20 cm center area and a
212 periphery. The peripheral area was further divided into middle (inner 10 cm) and an outer area
213 (outer 10 cm) to determine thigmotaxic behavior. Mice were placed in the center and allowed to

214 explore the area freely for 15 min. Locomotion parameters such as total distance, velocity,
215 angular velocity and immobility were measured. Frequency and time duration in the center,
216 periphery and outer area were recorded to determine anxiety-like behavior. In addition, data were
217 nested into 5-min bins and distance moved during each of these 3 periods was recorded to
218 evaluate habituation differences across groups.

219 Novel Object: This assay was conducted 24 hours following the open field test in the same arena.
220 Each subject mouse was placed in the chamber containing two identical objects and allowed free
221 exploration for 10 minutes. Following a 3 hour delay, one of the familiar objects was replaced
222 with a novel object and the test mice were returned to the same arena. The time spent sniffing
223 each object was measured. Tester was blinded to the genotypes of tested mice. We scored and
224 reported raw data of time spend sniffing novel (NO) vs. habituated object (HO) Mice that did not
225 sniff either object and/or did not sniff for a total of 4 seconds were excluded from the final
226 analysis.

227 Olfactory Assay: Buried Food Retrieval. Mice were food deprived overnight and places in
228 standard clean cages with normal cage bedding (3 cm). Mice were allowed to acclimate for 5
229 minutes, then were removed to another clean cage at which point a uniform piece of food (Teddy
230 Graham) was placed in a random corner under approximately 1cm of normal bedding. Next, each
231 mouse was returned to its cage and the time to retrieve the food source (latency) was recorded.

232 Contextual and Cued Fear Conditioning: Fear conditioning test was conducted as the last
233 behavioral test in the series of all behavioral assesments. Experiments utilized two standard
234 conditioning chambers, each housed in an isolation cubicle and equipped with a stainless-steel
235 grid floor connected to a solid-state shock scrambler. Each scrambler delivered an electronic
236 constant-current shock source that was controlled via an interface connected to a Windows XP

237 computer running FreezeFrame software (Coulbourn Instruments, Allentown, PA). A digital
238 camera was mounted to the side of each chamber, and video signals were sent to the same
239 computer for analysis. During training, mice were placed in the conditioning chamber for 12 min
240 and then received four footshocks (cond. stimulus: 85 dB sound at 2800 Hz for 30 sec.;
241 unconditioned stimulus (US: 0.56mA). Retention test was performed 18 hrs later for 5 minutes in
242 the absence of a shock.

243 **Analysis of progenitor proliferation.** Mice received a single intraperitoneal injection of BrdU
244 (50 mg/kg, Sigma-Aldrich B5002) at E14.5 and sacrificed exactly 30 minutes later (veh.treated:
245 $n_{WT} = 8$, $n_{Del}=6$; inh.treated: $n_{WT} = 9$, $n_{Del}=9$). Sections were immunostained with anti-BrdU
246 antibody, (rat-anti-BrdU; 1:100, Abcam), or mouse anti-BrdU (1:100, BD Biosciences). The
247 number of BrdU+ cells per cortical sections (proliferative fraction) was established using
248 stereological technique and all positive cells within a 100 μ m segment along the ventricular
249 surface, extending from the ventricle to the pial surface, were counted. All data collection was
250 blinded to the genotype and randomized. In embryonic brains all analyses were performed at the
251 rostro-caudal axis of fully emerged ganglionic eminences, (LGE as well as MGE). These
252 structures as well as the presence of choroid plexus were noted and the images were taken just
253 above the pallial/subpallial boundary in the VZ as well dorso-medial area of the VZ. In adult
254 mice we evaluated BrdU staining in two different areas; 1) above the pallial/subpallial boundary
255 (dorsolateral), the other (2) at the level of dorsomedial cortex. For postnatal analyses we
256 evaluated both motor and somatosensory cortex.

257 **Microscopy and image analysis.** All sections were imaged using a Zeiss LSM 510 confocal
258 laser microscope equipped with argon and helium–neon lasers and analyzed with LCS confocal
259 software, Prism and Photoshop (Adobe). All counts were performed on blinded sections and

260 **two-way ANOVA with Bonferroni post hoc** was used to establish statistical significance for each
261 experiment.

262 **Western analysis.** Cortices were dissected from E14.5 embryos and washed with ice-cold
263 HBSS. The lysates were sonicated in lysis buffer (20 mM Tris, pH 7.5, 150 mM NaCl, 1% NP-
264 40, 10% glycerol, 1 mM EDTA, 1.5 mM MgCl₂, 20 mM NaF, and 20 mM β -glycerophosphate)
265 in the presence of protease inhibitors (1 μ g/ml leupeptin, 1 μ g/ml aprotinin, 1 mM PMSF, and
266 1 mM Na₃VO₄). Samples were centrifuged, and protein concentrations were established with
267 bicinchoninic acid assay (Pierce) using a BSA standard. Equal amounts of protein were boiled in
268 sample buffer, separated on SDS-PAGE gels, and transferred to Immobilon-P polyvinylidene
269 difluoride membranes (Millipore). Membranes were blocked in 3% BSA (or 5% skim-milk) in
270 TBS and 0.1% Tween 20 (TBS-T) for 2 h at room temperature and incubated with primary
271 antibodies overnight at 4°C. The primary antibodies used were: rabbit anti-pERK (Cell
272 Signaling, 1:1000), mouse anti-ERK2 (BD Biosciences Discovery Labware, 1:3000), mouse
273 anti-ERK1 (Zymed Laboratories, 1:1000), anti-CoxIV and (1:3000; Cell Signaling). Membranes
274 were washed with TBS-T, incubated with HRP-conjugated secondary antibodies: goat anti-
275 mouse or anti-rabbit (1:5000; GE Healthcare) in TBS-T with 5% milk for 2 h at room
276 temperature. Detection was performed using Millipore chemiluminescence using BioMax MR
277 X-ray film (Eastman Kodak). Densitometry was performed using Adobe Photoshop histogram
278 function, and statistical analysis was done with GraphPad Prism software.

279 **ELISA.** The oxytocin (OT) Elisa was performed using ENZO Oxytocin kit (Prod.No. ADI-901-
280 153A) according to the manufactures instructions. Whole brain homogenates of P90 WT and
281 *16p11.2del* brains were used and the calometric readout was reported in pg/ml.

282 **Immunohistochemistry.** The E14.5 brains were dissected in cold PBS and fixed by immersion

283 in 4% paraformaldehyde (PFA) for 1 hour or overnight at 4° C. P10 and adult mouse brains were
284 fixed in 4% PFA/1X PBS at 4°C overnight and serially incubated in 10, 20 and 30% sucrose.
285 The brains were sectioned (10 μm), then rehydrated in PBS for 10 min. Antigen retrieval using
286 1X Reveal Decloaker (Biocare) was performed for 10 minutes at 95°C. Sections were blocked in
287 10% (embryonic) and 2% (postnatal) normal goat or donkey serum for 1 hour at room
288 temperature with 0.1% (vol/vol) Triton X-100 in PBS. Slides were incubated with primary
289 antibodies overnight at 4°C, rinsed with PBS and incubated with corresponding secondary
290 antibodies for 1-2 hours at room temperature. The primary antibodies used were as follows:
291 polyclonal rabbit anti-pERK (Cell Signaling, 1:100); rabbit polyclonal anti-Pax6 (Covance,
292 1:300); mouse anti-PH3 (Upstate, 1:250); rabbit anti-PH3 (Upstate, 1:500); rabbit anti-Tbr1
293 (Chemicon, 1:1000); rabbit anti-Tbr2 (1:300); chicken anti-Tbr2 (1:250); goat anti-Brn1 (Santa
294 Cruz Biotechnology, 1:50), rat anti-Ctip2 (Abcam, 1:500); rabbit anti-Cux1 (Santa Cruz, 1:100)
295 and mouse anti-SatB2 (Abcam, 1:100). Secondary antibodies used were Alexa Fluor 488
296 (1:1000), 546 or 593 (1:1000) conjugated to goat or donkey anti-mouse, anti-rabbit or anti-goat
297 (Invitrogen). DNA was stained with 4',6'-diamidino-2-phenylindole (DAPI) for 5 min
298 (DAPI, Molecular Probes). Immunohistochemical staining was performed on all 4 groups
299 simultaneously.

300 ***Embryonic Brains.*** Anatomically matched sections of littermate WT and mutant mice were
301 analyzed. At least **3 consecutive** sections per animal were analyzed alongside the mid-rostro-
302 caudal axis of the dorsal telencephalon. Embryonic coronal sections were evaluated at the level
303 of the ganglionic eminences and analyzed by counting all cells in standard 100μm **bins extending**
304 **from the ventricle to the pial surface.** Quantification was performed blind to genotype as
305 previously described (Glickstein et al., 2009). **Three to four litters were examined per**

306 **experiment.**

307 **Adult Brains.** We counted at least three consecutive tissue slices per slide and at least four slides
308 per animal. In postnatal brains, coronal sections were used to count cells in 400 μ m boxes in
309 somatosensory and motor cortex. Slides were picked at random and the investigator was blinded
310 to genotypes and treatments. All data from a single experiment, incorporating all 4 experimental
311 groups, was averaged. The number of mice evaluated is indicated in figure legends, with **three to**
312 **four litters examined per experiment.**

313 **Statistical Analysis.** All data analyzed followed normal distribution according to the
314 Kolmogorov-Smirnov test. Statistical significance was determined using two-way ANOVA
315 followed by Bonferroni's post hoc test for multiple comparisons. Data analysis was performed
316 using GraphPad Prism and presented as means \pm s.e.m.

317 All experiments in this study were blinded and randomized. All mice bred for the
318 experiments were utilized for preplanned experiments and randomized to experimental groups.
319 Visibly sick animals were excluded before data collection and analysis. Data were collected,
320 processed and analyzed randomly. The experimental design, treatments and handling of mice
321 were identical across experiments. Littermates were used as controls with multiple litters (3-4)
322 examined per experiments. All mice (including the MRI study) were bred in the Case Western
323 Reserve Animal Core.

324 **Results:**

325 **Pharmacological Normalization of ERK Activity with an ERK Pathway Inhibitor in**
326 **16p11.2del Mice.**

327 In order to test our hypothesis that there are ERK-mediated pathologic processes
328 occurring in the *16p11.2del* mice, we took advantage of two recently developed brain penetrant

329 peptides, RB1/RB3, which act in concert to attenuate Ras-ERK activity in the brain(Papale et al.,
330 2016, 2017). These brain penetrant peptides exhibit IC50 values in the micromolar range (Papale
331 et al., 2016). Importantly, these peptides have been successfully used *in vivo* for early post-natal
332 developmental treatments, manifesting a remarkable high degree of tolerability and low toxicity.
333 Based on these promising results, we treated with the RB1/RB3 mix (hereafter termed ‘ERK
334 Inhibitor’) the pregnant *16p11.2del* carrier dams for 5 consecutive days starting at E10.5,
335 encompassing a critical period of cortical neurogenesis. We observed that the enhanced ERK
336 activity in dorsomedial cortex of *16p11.2del* mice at E14.5 was normalized in the inhibitor-
337 treated mice (Fig. 1a,b,c). At E14.5 two-way ANOVA analysis of ERK1 activity showed a
338 significant effect with respect to genotype ($F[1,59]=21.7$, $p<0.0001$) and inhibitor treatment
339 ($F[1,59]=10.12$, $p=0.002$), but with an interaction between both variables ($F[1,59]=4.05$,
340 $p=0.049$). Bonferonni post-hoc analysis showed a 2-fold increase in ERK1 activity ($p<0.0001$) in
341 the vehicle treated *16p11.2del* mice compared to vehicle treated WT mice that normalized to WT
342 levels following inhibitor treatment. Similarly, ERK2 activity was also significantly affected by
343 both genotype ($F[1,77]=4.31$, $p=0.041$) and inhibitor treatment ($F[1,77]=6.76$, $p=0.011$) when
344 analyzed by two-way ANOVA, however a significant interaction between genotype and drug
345 treatment was present ($F[1,77]=5.08$, $p=0.027$). A Bonferonni post-hoc analysis showed a 49%
346 ($p=0.017$) increase in ERK2 activity in the vehicle treated *16p11.2del* mice compared to vehicle
347 treated WT mice that normalized to WT levels with inhibitor treatment. Importantly, total ERK1
348 levels were reduced in the *16p11.2del* mice in both vehicle and inhibitor treated animals, with a
349 significant genotype effect observed by two-way ANOVA ($p<0.0001$). We observed significant
350 interactions between the inhibitor and genotype because, interestingly, the dose of the ERK
351 inhibitor (10 mg/kg, i.p.) used in our studies did not alter ERK activity in the WT littermates. In

352 addition, when ERK1/2 activity was analyzed in P10 embryonically treated mice (Fig. 1d,e),
353 there was an inhibitor effect (pERK1:p=0.005, pERK2:p=0.017) by two-way ANOVA, with a
354 Bonferonni post-hoc analysis showing a 75% (p<0.01) and 62% (p<0.01) increase in ERK1 and
355 ERK2, respectively, in the *16p11.2del* vehicle treated mice that normalized to WT levels. Thus, a
356 prenatal treatment of embryonic mice resulted in abrogation of abnormal ERK hyperactivity in
357 the developing cortex when examined at E14.5 (Fig. 1b,c) or postnatally at P10 (Fig. 1d, e).

358

359 **ERK Inhibitor Treatment Rescues Embryonic and Postnatal Cortical Defects in the** 360 ***16p11.2del* Mice.**

361 Next, we investigated whether the embryonic treatment with the ERK pathway inhibitor
362 could correct aberrant progenitor proliferation dynamics in the developing cortex (Fig. 2 a-b) and
363 rescue deficits in cortical neurogenesis (Fig. 2c-d). We evaluated the number of proliferating,
364 BrdU+ progenitors following a single, 30 min IP BrdU injection at E14.5. A 2-way ANOVA
365 analysis showed no genotype or inhibitor effect, but Bonferroni post-hoc analysis showed a 30%
366 increase (p<0.05) in BrdU+ progenitors in the vehicle treated *16p11.2del* mice compared to
367 vehicle treated WT mice. This increase in progenitor proliferation was abrogated in ERK
368 inhibitor treated *16p11.2del* mice and returned to WT levels (Fig.2a). Furthermore, western blot
369 analysis and immunohistochemistry (IHC) demonstrate that the number of Tbr2+ intermediate
370 progenitor cells (IPCs) residing in the SVZ can be restored to normal levels after the inhibitor
371 treatment (Fig. 2b). Western blot analysis of Tbr2 by two-way ANOVA showed a genotype and
372 inhibitor interaction, but post-hoc analysis revealed a 30% decrease in Tbr2 levels (p<0.0001) in
373 the vehicle *16p11.2del* mice, which returned to normal following treatment, when compared to
374 vehicle WT mice. This correlated with a 37% decrease (post-hoc Bonferroni, p=0.0012) in the

375 number of Tbr2⁺ cells by IHC in the vehicle treated *16p11.2del* mice, that corrected to WT
376 levels in the inhibitor treated mice when compared to vehicle WT animals (2-way ANOVA
377 showed significant inhibitor and genotype interaction). Additionally, using western analysis and
378 IHC we also show that treatment with ERK inhibitor ameliorates the aberrant elevation of the
379 number of early born cortical neurons marked by Ctip2⁺ and Tbr1⁺ that populate cortical layer
380 V and VI, respectively (Fig.2c-d). Again 2-way ANOVA analyses of IHC and western blots of
381 Tbr1 and Ctip2 showed interactions between genotype and inhibitor, but the post-hoc Bonferroni
382 analysis showed a 50% increase in Ctip2 levels (p=0.012) and a 30% increase in Ctip2⁺ cells by
383 IHC (p=0.0005) in the *16p11.2del* vehicle treated mice, which returned to WT levels when
384 compared to WT vehicle treated animals. Tbr1 analysis showed a 35% increased in Tbr1 protein
385 levels (p=0.038), and a 20% increase in Tbr1⁺ cells via IHC (p=0.025) in the *16p11.2del* vehicle
386 treated mice that returned to WT levels in the inhibitor treated mice, when compared to WT
387 vehicle treated animals.

388 Next, we tested whether prenatal ERK inhibitor treatment resulted in permanent rescue of
389 cortical cytoarchitecture defects by evaluation of postnatal mice at P2. We show that the number
390 of Brn1⁺ and Satb2⁺ layer II-III pyramidal neurons is restored to normal levels after prenatal
391 ERK inhibitor treatment (Fig.3a-b). These are cortico-cortical connections, some of which
392 project to contralateral hemisphere across the corpus callosum (O'Rourke et al., 1995). Satb2
393 analysis shows significant genotype (p=0.048) and treatment effect (p=0.013) by 2-way
394 ANOVA. Post-hoc analysis shows significant 13% reduction in Satb2⁺ cells in vehicle deletion
395 animals compared to WT vehicle (p=0.03), which is abrogated with inhibitor treatment of
396 deletion animals, which show Satb2⁺ cells similar to vehicle WT animals and significant
397 increase when compared to vehicle treated *16p11.2del* mice (p=0.01). Brn1 analysis shows no

398 genotype or treatment effect by 2-way ANOVA, but post-hoc analysis shows decrease Brn1+
399 cells in vehicle treated *16p11.2del* mice compared to WT vehicle-treated animals (p<0.05), but
400 inhibitor treated *16p11.2del* mice show no difference in Brn1+ cells compared to WT vehicle-
401 treated animals.

402 Analysis of Tbr1 cells by 2-way ANOVA showed an interaction between genotype and
403 inhibitor treatment, but post-hoc analysis of vehicle treated *16p11.2del* animals showed a 25%
404 increase in Tbr1+ cells compared to vehicle treated WT animals (post-hoc Bonferroni,
405 p=0.0075), which is rescued with treatment of *16p11.2del* animals with ERK inhibitor (Fig. 3d),
406 consistent with the effect of the inhibitor on these neurons observed at E14.5 (Fig.2d). **The**
407 **number of Ctip2+ layer V neurons, known to project to sub-cortical targets including the**
408 **thalamus, midbrain, pons and spinal cord, is increased during mid-neurogenesis, but decreased**
409 **postnatally in vehicle 16p11.2del mice when compared to WT vehicle treated mice** (post-hoc
410 Bonferroni, p =0.014) and normalized by inhibitor treatment of *16p11.2del* animals, which have
411 more Ctip2+ neurons compared to vehicle *16p11.2del* animals (p=0.033) and no difference
412 compared to WT vehicle treated animals (Fig.2c, 3c). It is unknown why these projection
413 neurons are ultimately lost in the *16p11.2del* mice. These data demonstrate the developmental
414 rescue of cortical deficits in progenitor proliferation and neurogenesis in the *16p11.2del* after
415 pharmacological intervention with the ERK pathway inhibitor.

416

417 **ERK inhibitor treatment normalizes levels of the cell cycle regulators p27^{Kip1} and cyclin**
418 **D1.**

419 To examine whether the aberrant generation of cortical neurons is due to deficits in cell
420 cycle dynamics, we examined two critical cell cycle regulators: p27^{Kip1} and cyclin D1 (Fig.4),

421 which are directly regulated by ERK signaling and play an important role in progenitor
422 proliferation (Calegari and Huttner, 2003; Dehay and Kennedy, 2007; Lange et al., 2009;
423 Pucilowska et al., 2012). We performed IHC and western blot analysis and observed a significant
424 decrease in p27^{Kip1} protein levels in the *16p11.2del* cortex, consistent with our previous
425 observations. Two-way ANOVA analysis of p27^{Kip1} showed no genotype or inhibitor effect, but
426 post-hoc analysis showed a 31% decrease ($p < 0.01$) in p27^{Kip1} levels in the *16p11.2del* vehicle
427 treated mice compared to the WT vehicle treated animals, which normalized to 92% of the
428 vehicle WT level after inhibitor treatment (Fig. 4b'-b"). When cyclin D1 levels were analyzed
429 by two-way ANOVA, there was only a inhibitor effect ($F[1,46], p < 0.0001$), but no genotype
430 effect, with significant decrease in cyclin D1 in the inhibitor treated *16p11.2del* mice ($p < 0.001$)
431 compared to the vehicle treated *16p11.2del* mice (Fig. 4a-a"). These data show that the
432 *16p11.2del* mice exhibit ERK dependent changes in cell-cycle dynamics of neural progenitor
433 cells that are ameliorated with the prenatal ERK inhibitor treatment.

434

435 **ERK inhibitor treatment partially rescues hippocampal and septal morphoanatomical** 436 **abnormalities in *16p11.2del* mice**

437 To determine whether ERK inhibitor treatment would affect macroscale brain
438 morphoanatomy in *16p11.2del* mice, we applied voxelwise Tensor Based Morphometry (TBM)
439 and automated anatomical labeling to high-resolution MRI brain scans (Pagani et al., 2016).
440 Consistent with previous reports (Horev et al., 2011), *16p11.del* mice showed increases in the
441 relative volume of the hypothalamus, superior colliculus and periaqueductal grey when
442 compared to control (WT) mice (Fig. 5a). Voxelwise TBM mapping also revealed foci of
443 decreased volume in ventral hippocampal, amygdalar, entorhinal and lateral septal areas in

444 *16p11.2del* mice when compared to WT controls (Fig.5a). Importantly, treatment with the ERK
445 inhibitor partially-rescued ventral hippocampal and lateral septal volume in *16p11.2del* mice
446 when compared to vehicle treated controls (Fig. 5b-c). Interestingly, the ventral hippocampus is
447 a region where pERK is highly expressed during mid-neurogenesis and a key substrate for
448 anxiety-related behavior (Kjelstrup et al., 2002; Maren and Holt, 2004) which these mice exhibit.

449

450 **Rescue of behavioral deficits in *16p11.2del* mice after prenatal ERK inhibitor treatment.**

451 We, as well as others, have previously shown that the *16p11.2del* mice are smaller than
452 their WT littermates (Horev et al., 2011; Portmann et al., 2014; Pucilowska et al., 2015; Tidyman
453 and Rauen, 2016). We report that prenatal treatment with ERK pathway inhibitor restored
454 normal body weight in the *16p11.2del* mice when examined at 3 months of age (WT vehicle
455 treated: 35.015g; *16p11.2del* vehicle treated: 25.352g; *16p11.2del* inhibitor-treated: 29.396g).

456 The *16p11.2 del* mice are reported to exhibit many behavioral deficits (Horev et al.,
457 2011; Portmann et al., 2014; Pucilowska et al., 2015; Yang et al., 2015). We tested the
458 *16p11.2del* and WT control mice in a number of standard behavioral paradigms that are altered
459 by the *16p11.2* deletion. Specifically, we assayed open field to evaluate hyperactivity and
460 anxiety-like behaviors, novel object and fear conditioning to examine hippocampal dependent
461 memory, elevated-plus maze (EPM) to test anxiety as well as maternal behavior and olfaction.
462 We evaluated three large cohorts (n=30/genotype) of 3 month-old male mice (except for
463 maternal behavior and olfaction). Data was analyzed by 2-way ANOVA, but unless otherwise
464 indicated, significant interaction occurred between the genotype and inhibitor treatment, which
465 resulted in reliance on post-hoc analysis to show genotype or inhibitor effects.

466 **We first conducted the EMP test**, where examining entries into the closed arm, the post-

467 hoc analysis showed fewer closed arm entries by vehicle *16p11.2del* mice compared to vehicle
468 WT mice ($p<0.05$), which was rescued in the inhibitor treated deletion animals who showed
469 more closed arm entries compared to vehicle treated *16p11.2del* animals ($p<0.05$) and no
470 difference with vehicle treated WT animals. Furthermore, we observed statistical significance in
471 time spent in the open arm ($p<0.05$), which was only partially rescued by inhibitor treatment
472 with no genotype or inhibitor effect by 2-way ANOVA. We also noted an increase in open arm
473 immobility, indicating freezing behavior (6a). In the open field test (Fig. 6b), we first examined
474 level of activity which showed that the *16p11.2del* mice did not explore the field as much as the
475 WT mice. 2-way ANOVA analysis of total distance travelled showed significant genotype
476 ($F[1,76]$, $p=0.005$) and drug effect ($F[1,76]$, $p=0.02$) with no interaction, although post-hoc tests
477 did not show significance between vehicle WT and *16p11.2del* animals or vehicle and inhibitor
478 treated *16p11.2del* animals. However, in the open field test (Fig. 6b), we observed that vehicle
479 treated *16p11.2del* mice spent more time in the center compared to vehicle treated WT mice
480 (post-hoc Bonferroni, $p<0.01$), which was rescued by ERK inhibitor treatment, as inhibitor
481 treated *16p11.2del* mice were similar to vehicle treated WT mice and spent less time in the
482 center compared to the vehicle treated *16p11.2del* mice (post-hoc Bonferroni, $p<0.05$).
483 Interestingly, total distance travelled was also increased in the vehicle treated *16p11.2del* mice
484 compared to vehicle treated WT mice (post-hoc Bonferroni, $p<0.05$), which again normalized
485 with inhibitor treatment of *16p11.2del* mice, who showed significant decreased in distance
486 travelled compared to vehicle treated *16p11.2del* n animals ($p<0.05$) and no difference with
487 vehicle treated WT animals.

488 Contextual fear conditioning showed significantly higher freezing percentage in the
489 vehicle treated *16p11.2del* mice compared to the vehicle treated WT cohort (post-hoc

490 Bonferroni, $p < 0.01$) indicating impaired contextual memory (Fig. 6c). This is improved by
491 treatment of the *16p11.2del* animals with the ERK inhibitor, which show no difference
492 compared to vehicle treated WT animals, but no significant difference was observed between
493 vehicle and inhibitor treated *16p11.2del* animals.

494 Novel object recognition (NOR) did not reveal a significant genotype or inhibitor effect
495 in post-hoc analysis, but a trend showing impaired NOR in vehicle treated *16p11.2del* compared
496 to vehicle treated WT mice ($p = 0.16$), which improved with inhibitor treatment of *16p11.2del*
497 mice, who showed a trend toward improvement in NOR compared to vehicle treated *16p11.2del*
498 mice ($p = 0.11$) (Fig 6d).

499 Both male and female *16p11.2del* mice exhibited a significantly higher acuity in their
500 sense of smell compared to the WT mice (post-hoc Bonferroni, $p < 0.01$), which was attenuated
501 after the treatment (Fig 6f). Inhibitor treated *16p11.2del* mice showed significant attenuation in
502 olfaction compared to vehicle treated *16p11.2del* mice ($p < 0.0001$).

503 Additionally, females showed heightened maternal response, as measured in a pup
504 retrieval assay that was reduced following ERK inhibitor treatment (Fig. 6e). Vehicle treated
505 *16p11.2del* animals showed decreased latencies to retrieving all pups compared to vehicle
506 treated WT animals (pup1: $p < 0.01$, pup2: $p < 0.01$, pup3: $p < 0.001$). This effect was reverted with
507 treatment of *16p11.2del* animals with inhibitor as no difference in latencies was observed when
508 compared to WT vehicle treated animals (post-hoc Bonferroni, $p < 0.01$).

509 Altogether, the above evidence supports the notion that an early pharmacological
510 intervention targeting ERK signaling in *16p11.2del* mice is sufficient to reverse some of the
511 behavioral alterations found in this model of ASD.

512

513 **Postnatal treatment with ERK inhibitor partially restores behavioral deficits of adult**
514 ***16p11.2del* mice.**

515 We next questioned whether any of the behavioral deficits could be improved by ERK
516 inhibitor treatment in adult mice. Therefore, we treated 3 month-old WT and *16p11.2del* male
517 mice with ERK inhibitor for 5 consecutive days at P90.

518 In the elevated plus maze, we observed that vehicle treated *16p11.2del* animals spent
519 more time in the open arm compare to the vehicle WT cohort (Fig. 7a; post-hoc Bonferroni, p
520 <0.05). This effect was abrogated in ERK inhibitor treated *16p11.2del* animals as no difference
521 in open arm time was observed when compared to vehicle treated WT animals (2-way ANOVA
522 showed significant interaction between genotype and inhibitor treatment). In the open field test,
523 we did not observe significant genotype effects between vehicle treated *16p11.2del* and WT
524 animals in post-hoc analysis, however, we did observe a trend toward more open entries in
525 vehicle *16p11.2 del* animals compared to WT (Fig. 7b). In addition, treatment of *16p11.2del*
526 animals with the ERK inhibitor showed significant reduction in entries into the center of the field
527 compared to vehicle treated *16p11.2del* animals (post-hoc Bonferroni, $p<0.01$). Although the
528 adult treated mice did not achieve statistical significance in the olfactory test, there was a trend
529 toward heightened acuity in the *16p11.2del* mice, which was at least partially recovered after the
530 inhibitor treatment (Fig. 7d). Together our data suggests that post-natal treatment with the ERK
531 inhibitor may result in partial rescue of some of the behavioral deficits seen in the *16p11.2del*
532 mice.

533 Since other models linked to ASDs and the ERK pathway show aberrant levels of
534 oxytocin (Hollander et al., 2007), we examined 3 month-old male mice and show that levels of
535 oxytocin are elevated in the *16p11.2del* male mice and importantly can be restored to normal

536 after inhibitor treatment (post-hoc Bonferroni, $p < 0.01$) (Fig. 7c). We observed by 2-way ANOVA
537 a significant genotype ($F(1, 24) = 6.132$, $p = 0.0207$) and drug effect ($F(1, 24) = 8.712$, $p = 0.0070$)
538 and significant interaction $F(1, 24) = 4.884$, $p = 0.0369$.

539 The *16p11.2del* mice do not exhibit typical social deficits that are common among other
540 models of ASDs as well as *16p11.2del* patients, thus, the enhanced oxytocin levels, which
541 normally augment social interactions, could be masking the social impairment in these mice.
542 Further studies using oxytocin inhibitors could clarify this phenomenon.

543 **Discussion:**

544 *ERK/MAPK pathway as a potential target for ASD therapy*

545 The ERK/MAPK pathway has been extensively studied and found to play pivotal roles in
546 neural development as well as in learning, memory, synaptic plasticity and spine dynamics
547 (Thomas and Huganir, 2004). The functional importance of signaling through this pathway is
548 also reflected in the effects of activating mutations that alter the activity of the ERK1/2 kinases
549 and result in a constellation of syndromic and non syndromic neurodevelopmental disorders,
550 including the RASopathies and the associated intellectual disability (Tidyman and Rauen, 2016;
551 Borrie et al., 2017).

552 It has recently been appreciated that some forms of ASD are also associated with
553 perturbations of several intracellular signaling cascades, including the Ras-ERK and the
554 mTORC1 pathways (Kalkman, 2012; Adviento et al., 2014; Borrie et al., 2017). In addition to
555 genetic linkages, pathway network analyses point to a convergence of a wide range of
556 abnormalities associated with autism onto a few salient pathways, prominent amongst these is
557 the ERK/MAPK pathway (Wen et al., 2016; Mitra et al., 2017). Importantly, many ASD mouse
558 models with genetic alterations of *Mecp2*, *FMR1*, *NF1*, *Syngap* as well as, *BTBR* and

559 *16p11.2del* exhibit aberrant ERK signaling (Liang et al., 2010; Osterweil et al., 2010, 2013;
560 Hamdan et al., 2011; Bhakar et al., 2012; Wang et al., 2013; Golzio et al., 2012; Kelleher III et
561 al., 2012; Wang et al., 2012; Faridar et al., 2014; Pucilowska et al., 2015). These data argue that
562 the abnormal ERK activity in the brain is central to pathology of many ASDs.

563 We and others have previously shown that the genetic deletion of the *16p11.2* interval
564 results in a paradoxical increase in ERK activity that is associated with aberrant neural
565 progenitor proliferation which leads to dysregulation in the number of neurons generated within
566 the cortex (Pucilowska et al., 2015) and subcortical structures (Portmann et al., 2014; Grissom et
567 al., 2018). This results in altered volumes of the cortical lamina and subcortical nuclei.

568 These studies raise the possibility that ERK inhibitors can be used to normalize their
569 activity and have therapeutic efficacy in *16p11.2* deletion carriers. We reasoned that
570 normalization of ERK activity might rescue the CNS phenotypes observed in the *16p11.2del*
571 mice. It is noteworthy that Papale et al., utilizing the newly developed ERK pathway inhibitor
572 peptides, have recently shown that the treatment ameliorates defective synaptogenesis in a
573 genetic model of RASopathy (Papale et al., 2017). Moreover, they have shown its effectiveness
574 of ERK pathway inhibition by treatment of murine models of cocaine addiction, suppressing the
575 behavioral phenotypes (Papale et al., 2016).

576 *ERK inhibitor suppresses the increase in ERK activity in 16p11.2del mice*

577 The *16p11.2del* mice exhibit paradoxical increase in ERK activity in both the developing
578 and mature brain. This finding was unexpected given that the deletion removes the *Mapk3* gene
579 encoding ERK1. The biological basis of dysregulation of the ERK pathway in this model is
580 unknown. However, we and others have previously postulated that ERK1 acts a negative
581 regulator of ERK2 (Mazzucchelli et al., 2002; Vantaggiato et al., 2006; Fasano and Brambilla,

582 2011; Trabalzini and Retta, 2014) and our findings are consistent with this hypothesis but basis
583 of the elevated ERK1 activity remains unclear. We found that basal ERK activity in wildtype
584 mice was not altered by drug treatment and this likely represents the intrinsic basal activity of the
585 ERKs that is independent of upstream regulators, and thus not subject to further inhibition by the
586 RB1 peptide.

587 The *16p11.2* deletion contains 27 genes. Mice lacking ERK1 or ERK2 do not recapitulate
588 the entire range of defects observed in the *16p11.2del* mice, implicating the contribution of other
589 genes within this interval to the ASD phenotypes. Importantly, at least two other genes (*MVP*
590 and *KCTD13*) within the deleted region converge onto the MAPK pathway and affect cell
591 proliferation, mGluR5 signaling and protein turnover (Liang et al., 2010; Golzio et al., 2012;
592 Tian et al., 2015). This suggests that multiple genes within the deletion interval converge on the
593 ERK/MAPK pathway resulting in an overall increase in ERK activity.

594

595 *ERK inhibitor rescues cortical defects in 16p11.2del mice*

596 We provide mechanism-based evidence showing that treatment with ERK inhibitors
597 during the peak of neurogenesis rescues the structural and behavioral deficits observed in the
598 *16p11.2del* mice. Specifically, we found that the aberrant generation of cortical neurons was
599 restored to normal levels owing to normalization of neurogenesis following developmental drug
600 treatment. This was secondary to the ERK-dependent modulation of potent cell cycle regulators
601 cyclin D1 and p27^{Kip1}. The retention of normal numbers of neural progenitors during critical
602 neurogenic period allowed for generation of appropriate numbers of cells populating cortical
603 lamina as well as normal circuitry. Importantly, we corroborated our molecular and biochemical
604 findings with MRI data showing partial reversal of volumetric changes to the ventral

605 hippocampus and lateral septum. It is of interest to note that the MRI analyses showed that the
606 ERK inhibitor treatment did not rescue all of the anatomical abnormalities in the brain, which
607 may be related to a short treatment window implemented in this study and the temporal variation
608 in neurogenesis between different brain regions.

609 *ERK Inhibitor rescues behavioral deficits in 16p11.2del mice*

610 One of the most striking findings from this study is the reversal of a wide range of
611 behavioral deficits that arise from the *16p11.2* deletion. Our data shows the first developmental
612 rescue of ASD associated phenotypes in the *16p11.2del* mouse model. The data from the
613 elevated plus maze and open field did show statistical significance for changes in anxiety-like
614 behaviors but not as strong as in previous studies, which is possibly due to increased sample size,
615 longer handling habituation period and greater statistical rigor. However, we do observe
616 significant improvement in contextual fear memories in the inhibitor treated *16p11.2del* mice. It
617 is conceivable that the observed ventral hippocampal morphological rescue could explain the
618 inhibitor effect on anxiety-like behaviors and contextual memory, given the established roles of
619 these brain regions in emotional and stress coping responses (Kjelstrup et al., 2002; Bannerman
620 et al., 2003; Maren and Holt, 2004; Adhikari et al., 2011).

621 The strongest effects we found were in olfaction and maternal behaviors, where we
622 observed heightened responses in *16p11.2del* mice, which were attenuated with inhibitor
623 treatment. The decrease in latencies to retrieve pups and locate hidden food in the deletion mice
624 may represent enhanced sensory perception or processing, but may also reflect changes to neural
625 circuitry that govern motivational behavior.

626 Remarkably, we also report a partial rescue of the behavioral deficits by inhibitor
627 treatment of adult mice. This effect is likely due to the fact that ERK dysregulation persists into

628 adulthood in the *16p11.2del* animals (Pucilowska et al., 2015) and potentially disrupts the normal
629 role of ERK signaling in synaptic plasticity. At the synapse ERKs promote regulation of
630 translational mechanisms promoting protein synthesis and thus cognition (Thomas and Huganir,
631 2004). These synaptic changes ultimately lead to refinement of neuronal connectivity.
632 Furthermore, many mutations associated with ASDs converge on the ERK pathway impairing
633 cognitive functioning and adaptive behavioral plasticity (Komiyama et al., 2002; Levitt and
634 Campbell, 2009; Ebert and Greenberg, 2013). Correcting hyperactive ERK signaling in the adult
635 *16p11.2del* mice may thus lead to ameliorating of behavioral phenotypes that are mediated by
636 the post-natal functions of ERK signaling. Importantly, these data suggest that dysregulation of
637 ERK activity can be rescued during brain development through restoration of normal cortical
638 proliferation dynamics, and in adult mice, presumably due to the synaptic actions of the ERKs
639 previously described in this mouse model (Tian et al., 2015; Lu et al., 2018).

640 We show that normalization of ERK signaling in the *16p11.2del* mice can reverse the
641 molecular and behavioral phenotypes in the *16p11.2del* mice. While we observe significant
642 effects on neuronal population sizes, our analysis was restricted to cortical neurons and, given
643 that this is a germline hemideletion model, other areas of the nervous system are undoubtedly
644 affected. This is further supported by our imaging analysis that shows multiple brain regions that
645 are affected by the deletion. While we observe some behavioral improvements from post-natal
646 treatment with the ERK/MAPK inhibitor, further analysis of changes to neuronal morphology
647 and synaptic physiology in the *16p11.2del* mice is warranted to help characterize the post-natal
648 effects of the *16p11.2* deletion. Finally, we have only examined a few behavioral phenotypes and
649 gender differences in behaviors were not examined.

650 In conclusion, our findings lead to three important conclusions. Our data strongly

651 supports the hypothesis that ASDs are neurodevelopmental disorders affecting global brain
652 circuitry. Secondly, our work significantly strengthens the emerging hypothesis that multiple
653 disorders of impaired cognition and ASDs converge onto a few fundamental pathways, such as
654 the ERK/MAPK pathway, and affect a critical period of brain development. Finally, the
655 cognitive and neuropsychiatric symptoms of *16p11.2* microdeletion disorder are amenable to
656 targeted drug therapy, both during development and in the adult.

657

658

659 **References:**

660 Adhikari A, Topiwala MA, Gordon JA (2011) Single units in the medial prefrontal cortex with
661 anxiety-related firing patterns are preferentially influenced by ventral hippocampal activity.
662 *Neuron* 71:898–910 .

663 Adviento B, Corbin IL, Widjaja F, Desachy G, Enrique N, Rosser T, Risi S, Marco EJ, Hendren
664 RL, Bearden CE, Rauen KA, Weiss LA (2014) Autism traits in the RASopathies. *J Med*
665 *Genet* 51:10–20.

666 Avants BB, Tustison N, Song G (2009) Advanced normalization tools (ANTS). *Insight J* 2:1–35.

667 Bannerman DM, Grubb M, Deacon RMJ, Yee BK, Feldon J, Rawlins JNP (2003) Ventral
668 hippocampal lesions affect anxiety but not spatial learning. *Behav Brain Res* 139:197–213.

669 Bhakar AL, Dölen G, Bear MF (2012) The Pathophysiology of Fragile X (and What It Teaches
670 Us about Synapses). *Annu Rev Neurosci* 35:417–443.

671 Borrie SC, Brems H, Legius E, Bagni C (2017) Cognitive Dysfunctions in intellectual
672 disabilities: The contributions of the Ras-MAPK and PI3K-AKT-mTOR pathways. *Annu*
673 *Rev Genomics Hum Genet* 18:115–142.

674 Calegari F, Huttner WB (2003) An inhibition of cyclin-dependent kinases that lengthens, but
675 does not arrest, neuroepithelial cell cycle induces premature neurogenesis. *J Cell Sci*
676 116:4947–4955.

677 Cutuli D, Pagani M, Caporali P, Galbusera A, Laricchiuta D, Foti F, Neri C, Spalletta G,
678 Caltagirone C, Petrosini L, Gozzi A (2016) Effects of Omega-3 fatty acid supplementation
679 on cognitive functions and neural substrates: A voxel-based morphometry study in aged
680 mice. *Front Aging Neurosci* 8:38-52.

681 Dehay C, Kennedy H (2007) Cell-cycle control and cortical development. *Nat Rev Neurosci*
682 8:438–450.

683 Dorr AE, Lerch JP, Spring S, Kabani N, Henkelman RM (2008) High resolution three-
684 dimensional brain atlas using an average magnetic resonance image of 40 adult C57Bl/6J
685 mice. *Neuroimage* 42:60–69.

686 Ebert DH, Greenberg ME (2013) Activity-dependent neuronal signalling and autism spectrum
687 disorder. *Nature* 493:327–337.

688 Faridar A, Jones-Davis D, Rider E, Li J, Gobijs I, Morcom L, Richards LJ, Sen S, Sherr EH
689 (2014) Mapk/Erk activation in an animal model of social deficits shows a possible link to
690 autism. *Mol Autism* 5:57.

691 Fasano S, Brambilla R (2011) Ras-ERK Signaling in Behavior: Old Questions and New
692 Perspectives. *Front Behav Neurosci* 5:79.

693 Freedman TS, Sondermann H, Friedland GD, Kortemme T, Bar-Sagi D, Marqusee S, Kuriyan J
694 (2006) A Ras-induced conformational switch in the Ras activator Son of sevenless. *Proc*
695 *Natl Acad Sci* 103:16692–16697.

696 Ghebranious N, Giampietro PF, Wesbrook FP, Rezkalla SH (2007) A novel microdeletion at
697 16p11.2 harbors candidate genes for aortic valve development, seizure disorder, and mild
698 mental retardation. *Am J Med Genet A* 143A:1462–1471.

699 Glickstein SB, Monaghan JA, Koeller HB, Jones TK, Ross ME (2009) Cyclin D2 Is Critical for
700 Intermediate Progenitor Cell Proliferation in the Embryonic Cortex. *J Neurosci* 29:9614–
701 9624.

702 Golzio C, Willer J, Talkowski ME, Oh EC, Taniguchi Y, Jacquemont S, Reymond A, Sun M,
703 Sawa A, Gusella JF, Kamiya A, Beckmann JS, Katsanis N (2012) KCTD13 is a major
704 driver of mirrored neuroanatomical phenotypes of the 16p11.2 copy number variant. *Nature*
705 485:363–367.

706 Grissom NM, McKee SE, Schoch H, Bowman N, Havekes R, O’Brien WT, Mahrt E, Siegel S,
707 Commons K, Portfors C, Nickl-Jockschat T, Reyes TM, Abel T (2018) Male-specific
708 deficits in natural reward learning in a mouse model of neurodevelopmental disorders. *Mol*
709 *Psychiatry* 23:544–555.

710 Hamdan FF, Daoud H, Piton A, Gauthier J, Dobrzeniecka S, Krebs M-O, Joobor R, Lacaille J-C,
711 Nadeau A, Milunsky JM, Wang Z, Carmant L, Mottron L, Beauchamp MH, Rouleau GA,
712 Michaud JL (2011) De Novo SYNGAP1 Mutations in Nonsyndromic Intellectual Disability
713 and Autism. *Biol Psychiatry* 69:898–901.

714 Hanson E et al. (2015b) The cognitive and behavioral phenotype of the 16p11.2 deletion in a
715 clinically ascertained population. *Biol Psychiatry* 77:785–793.

716 Hollander E, Bartz J, Chaplin W, Phillips A, Sumner J, Soorya L, Anagnostou E, Wasserman S
717 (2007) Oxytocin increases retention of social cognition in autism. *Biol Psychiatry* 61:498–
718 503.

719 Horev G, Ellegood J, Lerch JP, Son Y-EE, Muthuswamy L, Vogel H, Krieger AM, Buja A,
720 Henkelman RM, Wigler M, Mills AA (2011) Dosage-dependent phenotypes in models of
721 16p11.2 lesions found in autism. *Proc Natl Acad Sci* 108:17076–17081.

722 Kalkman HO (2012) Potential opposite roles of the extracellular signal-regulated kinase (ERK)
723 pathway in autism spectrum and bipolar disorders. *Neurosci Biobehav Rev* 36:2206–2213.

724 Kelleher III RJ, Geigenmüller U, Hovhannisyanyan H, Trautman E, Pinard R, Rathmell B,
725 Carpenter R, Margulies D (2012) High-Throughput Sequencing of mGluR Signaling
726 Pathway Genes Reveals Enrichment of Rare Variants in Autism Esteban FJ, ed. *PLoS One*
727 7:e35003.

728 Kjelstrup KG, Tuvnes FA, Steffenach H-A, Murison R, Moser EI, Moser M-B (2002) Reduced
729 fear expression after lesions of the ventral hippocampus. *Proc Natl Acad Sci U S A*
730 99:10825–10830.

731 Komiyama NH, Watabe AM, Carlisle HJ, Porter K, Charlesworth P, Monti J, Strathdee DJC,
732 O’Carroll CM, Martin SJ, Morris RGM, O’Dell TJ, Grant SG (2002) SynGAP regulates
733 ERK/MAPK signaling, synaptic plasticity, and learning in the complex with postsynaptic

734 density 95 and NMDA receptor. *J Neurosci* 22:9721–9732.

735 Kumar RA, KaraMohamed S, Sudi J, Conrad DF, Brune C, Badner JA, Gilliam TC, Nowak NJ,
736 Cook EH, Dobyns WB, Christian SL (2007) Recurrent 16p11.2 microdeletions in autism.
737 *Hum Mol Genet* 17:628–638.

738 Lange C, Huttner WB, Calegari F (2009) Cdk4/CyclinD1 Overexpression in neural stem cells
739 shortens G1, delays neurogenesis, and promotes the generation and expansion of basal
740 progenitors. *Cell Stem Cell* 5:320–331.

741 Levitt P, Campbell DB (2009) The genetic and neurobiologic compass points toward common
742 signaling dysfunctions in autism spectrum disorders. *J Clin Invest* 119:747–754.

743 Levy D, Ronemus M, Yamrom B, Lee Y, Leotta A, Kendall J, Marks S, Lakshmi B, Pai D, Ye
744 K, Buja A, Krieger A, Yoon S, Troge J, Rodgers L, Iossifov I, Wigler M (2011) Rare De
745 Novo and Transmitted Copy-Number Variation in Autistic Spectrum Disorders. *Neuron*
746 70:886–897.

747 Liang P, Wan Y, Yan Y, Wang Y, Luo N, Deng Y, Fan X, Zhou J, Li Y, Wang Z, Yuan W, Tang
748 M, Mo X, Wu X (2010) MVP interacts with YPEL4 and inhibits YPEL4-mediated activities
749 of the ERK signal pathway. *Biochem Cell Biol* 88:445–450.

750 Liu S, Sun J-P, Zhou B, Zhang Z-Y (2006) Structural basis of docking interactions between
751 ERK2 and MAP kinase phosphatase 3. *Proc Natl Acad Sci* 103:5326–5331.

752 Lu H-C, Mills AA, Tian D (2018) Altered synaptic transmission and maturation of hippocampal
753 CA1 neurons in a mouse model of human chr16p11.2 microdeletion. *J Neurophysiol*
754 119:1005–1018.

755 Maren S, Holt WG (2004) Hippocampus and Pavlovian fear conditioning in rats: muscimol
756 infusions into the ventral, but not dorsal, hippocampus impair the acquisition of conditional
757 freezing to an auditory conditional stimulus. *Behav Neurosci* 118:97–110.

758 Marshall CR et al. (2008) Structural variation of chromosomes in autism spectrum disorder. *Am*
759 *J Hum Genet* 82:477–488.

760 Mazzucchelli C et al. (2002) Knockout of ERK1 MAP kinase enhances synaptic plasticity in the
761 striatum and facilitates striatal-mediated learning and memory. *Neuron* 34:807–820.

762 Mitra I, Lavillaureix A, Yeh E, Traglia M, Tsang K, Bearden CE, Rauen KA, Weiss LA (2017)
763 Reverse Pathway Genetic Approach Identifies Epistasis in Autism Spectrum Disorders Flint
764 J, ed. *PLOS Genet* 13:e1006516.

765 Newbern J, Zhong J, Wickramasinghe RS, Li X, Wu Y, Samuels I, Cherosky N, Karlo JC,
766 O’Loughlin B, Wikenheiser J, Gargasha M, Doughman YQ, Charron J, Ginty DD,
767 Watanabe M, Saitta SC, Snider WD, Landreth GE (2008) Mouse and human phenotypes
768 indicate a critical conserved role for ERK2 signaling in neural crest development. *Proc Natl*
769 *Acad Sci* 105:17115–17120.

770 O’Rourke NA, Sullivan DP, Kaznowski CE, Jacobs AA, McConnell SK (1995) Tangential
771 migration of neurons in the developing cerebral cortex. *Development* 121:2165–2176.

772 Osterweil EK, Chuang S-C, Chubykin AA, Sidorov M, Bianchi R, Wong RKS, Bear MF (2013)
773 Lovastatin corrects excess protein synthesis and prevents epileptogenesis in a mouse model
774 of fragile X syndrome. *Neuron* 77:243–250.

775 Osterweil EK, Krueger DD, Reinhold K, Bear MF (2010) Hypersensitivity to mGluR5 and
776 ERK1/2 leads to excessive protein synthesis in the hippocampus of a mouse model of
777 fragile X syndrome. *J Neurosci* 30:15616–15627.

778 Pagani M, Damiano M, Galbusera A, Tsiftaris SA, Gozzi A (2016) Semi-automated registration-
779 based anatomical labelling, voxel based morphometry and cortical thickness mapping of the

780 mouse brain. *J Neurosci Methods* 267:62–73.

781 Papale A, d’Isa R, Menna E, Cerovic M, Solari N, Hardingham N, Cambiaghi M, Corsi M,
782 Barbacid M, Leocani L, Fasano S, Matteoli M, Brambilla R (2017) Severe intellectual
783 disability and enhanced gamma-aminobutyric acidergic synaptogenesis in a novel model of
784 rare RASopathies. *Biol Psychiatry* 81:179–192.

785 Papale A, Morella IM, Indrigo MT, Bernardi RE, Marrone L, Marchisella F, Brancale A,
786 Spanagel R, Brambilla R, Fasano S (2016) Impairment of cocaine-mediated behaviours in
787 mice by clinically relevant Ras-ERK inhibitors. *Elife* 5. pii: e17111.

788 Portmann T et al. (2014) Behavioral abnormalities and circuit defects in the basal ganglia of a
789 mouse model of 16p11.2 deletion syndrome. *Cell Rep* 7:1077–1092.

790 Pucilowska J, Puzerey PA, Karlo JC, Galan RF, Landreth GE (2012) Disrupted ERK Signaling
791 during Cortical Development Leads to Abnormal Progenitor Proliferation, Neuronal and
792 Network Excitability and Behavior, Modeling Human Neuro-Cardio-Facial-Cutaneous and
793 Related Syndromes. *J Neurosci* 32:8663–8677.

794 Pucilowska J, Vithayathil J, Tavares EJ, Kelly C, Karlo JC, Landreth GE (2015) The 16p11.2
795 Deletion Mouse Model of Autism Exhibits Altered Cortical Progenitor Proliferation and
796 Brain Cytoarchitecture Linked to the ERK MAPK Pathway. *J Neurosci* 35:3190–3200.

797 Roskoski R (2012) ERK1/2 MAP kinases: Structure, function, and regulation. *Pharmacol Res*
798 66:105–143.

799 Sondermann H, Soisson SM, Boykevisch S, Yang S-S, Bar-Sagi D, Kuriyan J (2004) Structural
800 analysis of autoinhibition in the ras activator Son of Sevenless. *Cell* 119:393–405.

801 Sweatt JD (2004) Mitogen-activated protein kinases in synaptic plasticity and memory. *Curr*
802 *Opin Neurobiol* 14:311–317.

803 Thomas GM, Hagan RL (2004) MAPK cascade signalling and synaptic plasticity. *Nat Rev*
804 *Neurosci* 5:173–183.

805 Tian D, Stoppel LJ, Heynen AJ, Lindemann L, Jaeschke G, Mills AA, Bear MF (2015)
806 Contribution of mGluR5 to pathophysiology in a mouse model of human chromosome
807 16p11.2 microdeletion. *Nat Neurosci* 18:182–184.

808 Tidyman WE, Rauen KA (2009) The RASopathies: developmental syndromes of Ras/MAPK
809 pathway dysregulation. *Curr Opin Genet Dev* 19:230–236.

810 Tidyman WE, Rauen KA (2016) Pathogenetics of the RASopathies. *Hum Mol Genet* 25:R123–
811 R132.

812 Trabalzini L, Retta SF (2014) Ras signaling: methods and protocols. New York: Humana Press.

813 Ullmann JFP, Watson C, Janke AL, Kurniawan ND, Reutens DC (2013) A segmentation
814 protocol and MRI atlas of the C57BL/6J mouse neocortex. *Neuroimage* 78:196–203.

815 Vantaggiato C, Formentini I, Bondanza A, Bonini C, Naldini L, Brambilla R (2006) ERK1 and
816 ERK2 mitogen-activated protein kinases affect Ras-dependent cell signaling differentially. *J*
817 *Biol* 5(5):14.

818 Wang C-C, Held RG, Hall BJ (2013) SynGAP regulates protein synthesis and homeostatic
819 synaptic plasticity in developing cortical networks *PLoS One* 8:e83941.

820 Wang Y, Kim E, Wang X, Novitsch BG, Yoshikawa K, Chang L-S, Zhu Y (2012) ERK inhibition
821 rescues defects in fate specification of Nf1-deficient neural progenitors and brain
822 abnormalities. *Cell* 150:816-830..

823 Wen Y, Alshikho MJ, Herbert MR (2016) Pathway network analyses for autism reveal
824 multisystem involvement, major overlaps with other diseases and convergence upon MAPK
825 and calcium signaling. *PLoS One* 11:e0153329.

826 Worsley KJ, Evans AC, Marrett S, Neelin P (1992) A Three-Dimensional Statistical Analysis for
827 CBF Activation Studies in Human Brain. *J Cereb Blood Flow Metab* 12:900–918.
828 Yang M, Mahrt EJ, Lewis F, Foley G, Portmann T, Dolmetsch RE, Portfors C V., Crawley JN
829 (2015) 16p11.2 Deletion Syndrome Mice Display Sensory and Ultrasonic Vocalization
830 Deficits During Social Interactions. *Autism Res* 8:507–521.
831 Zufferey F et al. (2012) A 600 kb deletion syndrome at 16p11.2 leads to energy imbalance and
832 neuropsychiatric disorders. *J Med Genet* 49:660–668.
833
834

835

836

837

838

839

840

841

842

843

844

845

846

847

848

849

850

851

852

853 **Figure Legends:**

854

855 **Fig. 1 Rescue of ERK activity with an ERK pathway inhibitor in *16p11.2del* mice at E14.5**

856 **and P10. (a)** IHC of E14.5 coronal sections from mice treated with vehicle (veh) or ERK

857 inhibitor (inh). Veh treated *16p11.2del* mice shows upregulation of ERK activity in the

858 dorsomedial cortex * (anti-pERK; green). This is abrogated after 5 days of inhibitor treatment

859 starting at E10.5. **(b)** Western analysis of E14.5 veh or inh treated cortical lysates. **(c)**

860 Quantification of Western analysis showing a significant increase in ERK1 and ERK2 activity in

861 *16p11.2del* animals (pERK1, ****p<0.0001 and pERK2, *p<0.05), which is restored to normal

862 level after inhibitor treatment (## p=0.0087; # p<0.05) (veh.treated: nWT = 19, nDel=13;

863 inh.treated: nWT = 19, nDel=12). ERK1 total levels are decreased in vehicle deletion animals

864 (**p<0.01) and inhibitor animals (****p<0.0001) (veh.treated: nWT = 8, nDel=7; inh.treated:

865 nWT = 10, nDel=9) **(d)** Western analysis of P10 veh or inh treated cortical lysates **(e)** Western

866 analysis of P10 veh or inh prenatally treated cortical lysates, quantified in **(e)** ERK1 and ERK2

867 activity are elevated in deletion animals at P10 (pERK1 **p<0.01; pERK2, p**<0.01), which is

868 normalized in embryonic inhibitor treatment (#p<0.05, ####p<0.001). All values normalized to

869 loading control GAPDH or CoxIV and reported as a fold change. P values are from Bonferroni

870 post-hoc analysis (* compares WT to deletion, # compares vehicle deletion to inhibitor deletion).

871

872 **Fig. 2 Reversal of deficits in cortical neurogenesis in the *16p11.2del* mice after treatment**

873 **with ERK pathway inhibitor at E14.5.** Immunohistochemistry (IHC) of coronal sections and

874 western analyses of cortical lysates at E14.5 **(a)** IHC with proliferation marker, BrdU injected 30

875 min. prior to sacrifice. **(a')** The number of BrdU+ progenitors was analyzed (veh.treated: nWT =

876 8, nDel=6; inh.treated: nWT = 9, nDel=9); (*p<0.05, #p<0.05) . **(b)** IHC with intermediate

877 progenitor marker, Tbr2 (green). (b') Quantification of Tbr2+ progenitors (veh. treated: nWT =
878 11, nDel=4; inh.treated: nWT = 9, nDel=16) (**p<0.0012, ##p<0.0052). (b'') Quantification of
879 western analysis (veh.treated: nWT = 29, nDel=37; inh.treated: nWT = 23, nDel=21),
880 (***p<0.00001, #p<0.0388). (c) IHC for layer V marker, Ctip2 (red). (c') Quantification of
881 Ctip2+ neurons (veh. treated: nWT = 5, nDel=4; inh. treated: nWT = 4, nDel=6)(***p=0.0005,
882 #####p<0.0001, *p=0.026). (c'') Quantification of western analysis (veh treated: nWT=15,
883 nDel=9; inh treated nWT= 8, nDel=11), (*p=0.0186, ##p=0.0073). (d) IHC with layer VI
884 marker, Tbr1 (green). (d') Quantification of Tbr1+ neurons (veh.treated: nWT = 9, nDel=9;
885 inh.treated: nWT = 5, nDel=5) (*p=0.025, ####p=0.0004). (d'') Quantification of Western
886 analysis (veh. treated: nWT=15, nDel=7; inh treated: nWT= 11, nDel=12) (*p=0.038,
887 ##p=0.0017). All western analyses data represented as a fold change, normalized to a loading
888 control. P values are from Bonferroni post-hoc analysis (* compares WT to deletion, # compares
889 vehicle deletion to inhibitor deletion).

890

891 **Fig. 3 Prenatal treatment with an ERK pathway inhibitor stably restores normal cortical**
892 **cytoarchitecture *16p11.2del* mice.** (a) Mice were evaluated at P2 by IHC with layer II-IV
893 marker Brn1, (green). (a') Quantification of Brn1+ neurons shows a rescue in somatosensory
894 cortex of *16p11.2del* mice (veh treated: nWT=11, nDel=13; inh treated: nWT= 17, nDel=17)
895 (*p<0.05). (b) IHC with layer 2-4 marker, Satb2 (red). (b') Quantification of Satb2+ neurons.
896 (veh treated: nWT=14, nDel=13; inh treated: nWT= 10, nDel=15) (*p=0.033, #p=0.0105). (c)
897 IHC with layer V marker, Ctip2 (red). (c') Quantification of Ctip2+ neurons (veh treated:
898 nWT=21, nDel=14; inh treated: nWT= 9, nDel=13) (*p=0.014, #p=0.033). (d) IHC with layer VI
899 marker, Tbr1+ (green). (d') Quantification of Tbr1+ neurons (veh treated: nWT=8, nDel=9; inh

900 treated: nWT= 12, nDel=10) (**p=0.0076, #p=0.0535). P values are from Bonferroni post-hoc
901 analysis (* compares WT to deletion, # compares vehicle deletion to inhibitor deletion).

902

903 **Fig. 4 Treatment with ERK pathway inhibitor normalizes the levels of the downstream**
904 **ERK effectors: p27^{Kip1} and cyclin D1.** IHC of coronal sections and western analyses from WT
905 and *16p11.2del* mice at E14.5 (a) Immunostaining against CyclingD1 antibody (green), (a')
906 Western blot analysis, quantified in (a'') (veh treated: nWT=16, nDel=7; inh treated: nWT=16,
907 nDel=13) (**p<0.001); (b) Immunostaining against p27^{Kip1}(green), (b') Western blot analysis,
908 quantified in (b'') (veh treated: nWT=8, nDel=10; inh treated: nWT=8, nDel=10) (**p<0.01,
909 *p<0.05). P values are from Bonferroni post-hoc analysis.

910

911 **Fig. 5 Prenatal ERK inhibitor treatment partially rescues ventral hippocampal and**
912 **lateral septal volume in 16p11.2del mice.** Mice were treated for 5 consecutive days starting
913 at E10.5 and evaluated at P90. (a) TBM analyses revealed significant increased volume of SC,
914 PAG and Hypo in *16p11.2del* mice compared to WT littermates (*t*-test, $p < 0.01$ FWE cluster-
915 corrected, with cluster defining threshold of $|t| > 2.3$). In *16p11.2* deletion mice, we also
916 observed an increased volume of the RS ctx, as well as reduced volume of vHPC, LS, Ent ctx
917 and Amy (*t*-test, $p < 0.01$ FWE cluster-corrected, with cluster defining threshold of $|t| > 2.3$). (b)
918 Comparison between treated and non-treated *16p11.2del* mice shows that ERK-inhibitor
919 produces bilateral foci of increased volume in the vHPC and LS (*t*-test, $p < 0.01$ FWE cluster-
920 corrected, with cluster defining threshold of $|t| > 2.3$). (c) A composite illustration of panels (a)
921 and (b) revealed that foci of increased gray matter volume (red/yellow, from panel b) are
922 spatially located in the same hippocampal and septal regions exhibiting reduced gray matter

923 volume in 16p11.2 del mice (blu/light blue, from panel a), suggesting a partial anatomical rescue
924 of volumetric deficits upon treatment with ERK inhibitor. (d-e) Consistent with TBM results,
925 anatomical labelling revealed reduced relative volume in vHPC (t-test: $t_{17} = 3.78$, $p = 0.001$) and
926 LS (t-test: $t_{17} = 2.21$, $p = 0.041$) in *16p11.2del* mice compared to WT littermates (one-way
927 ANOVA of vHPC: $F_{3,34} = 8.083$, $p < 0.001$; one-way ANOVA of LS: $F_{3,34} = 1.692$, $p = 0.1872$).
928 Treatment with ERK inhibitor in *16p11.2del* mice partially restored morphoanatomical volume
929 in these brain regions (vHPC, t-test: $t_{16} = 2.79$, $p = 0.013$), although the effects in LS did not
930 reach full statistical significance (t-test, $t_{16} = 1.78$, $p = 0.078$). Amy, amygdala; Ent ctx,
931 entorhinal cortex; Hypo, hypothalamus; LS, lateral septum; PAG, periaqueductal grey; RS,
932 retrosplenial cortex; SC, superior colliculus; vHPC, ventral hippocampus. * $p < 0.05$, ** $p < 0.01$.

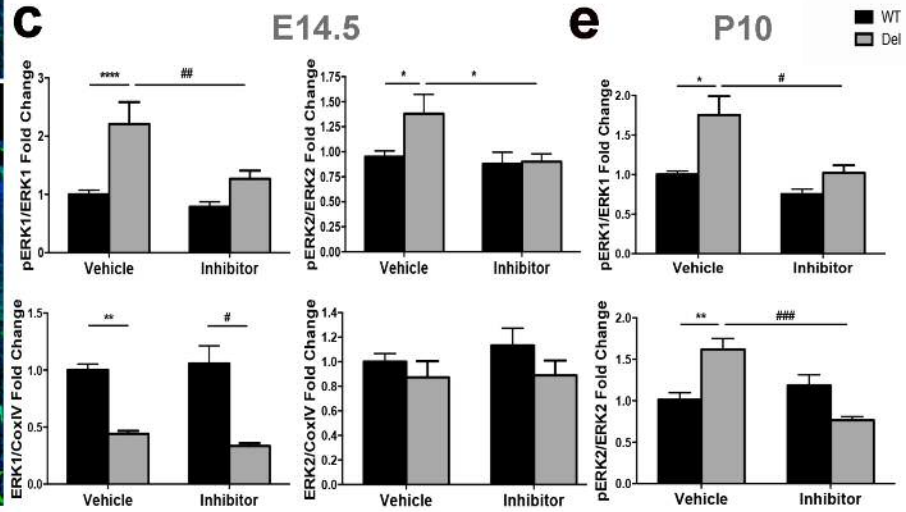
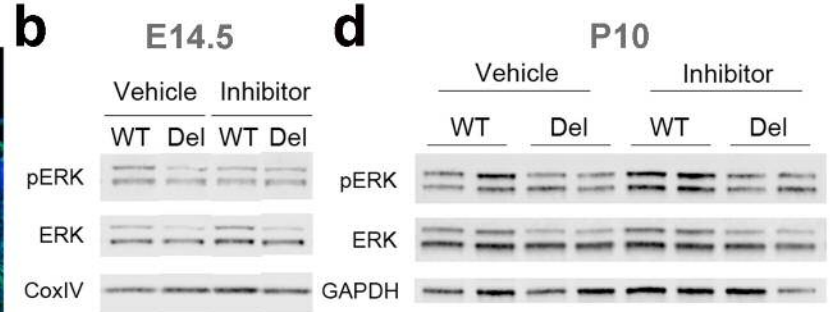
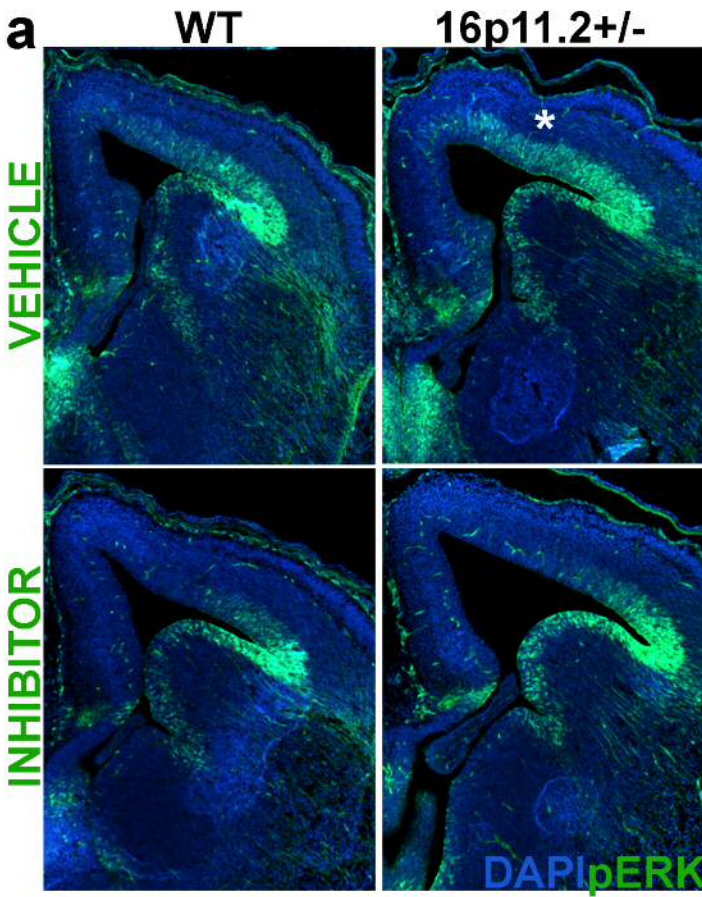
933

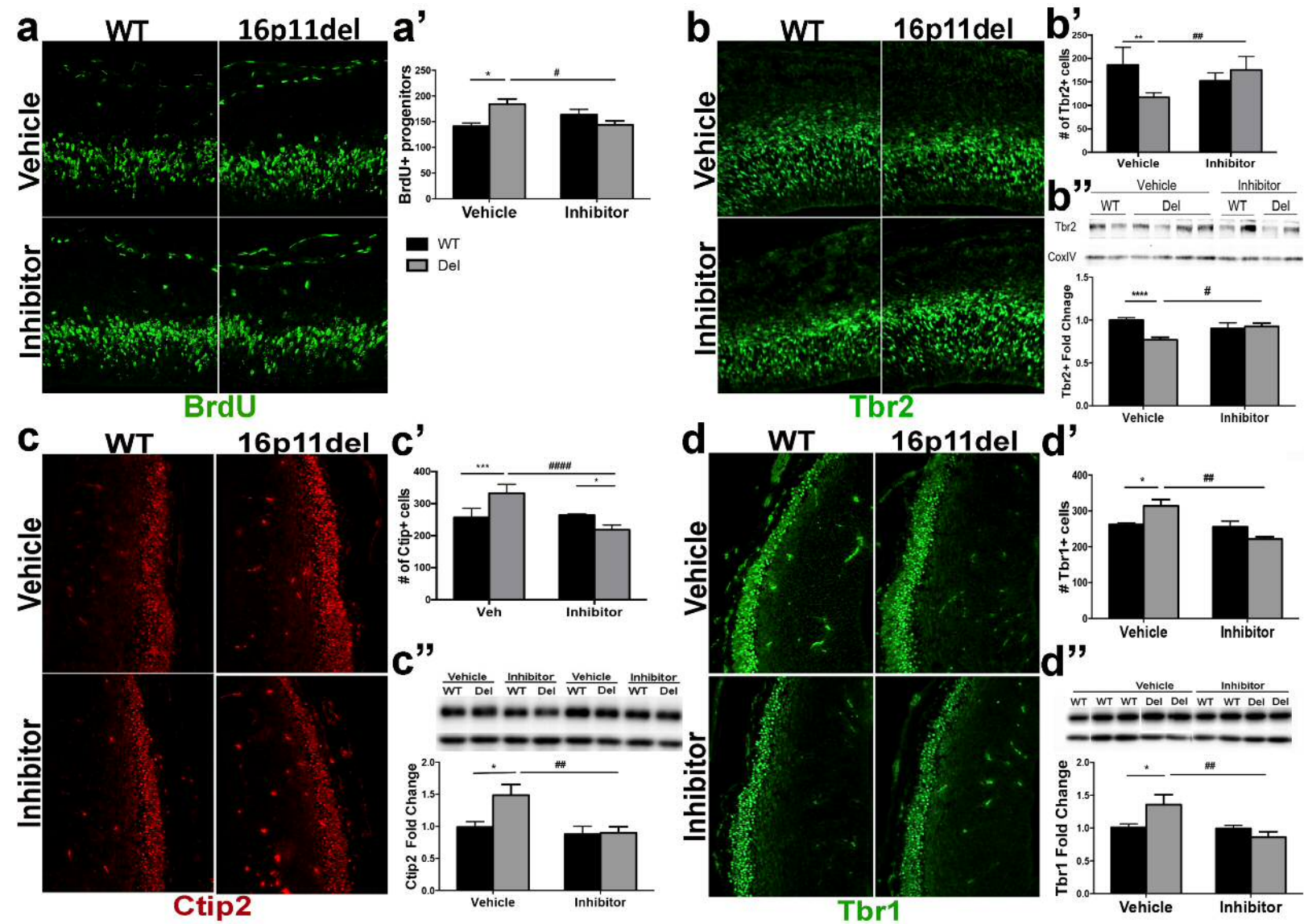
934 **Fig. 6 Reversal of Behavioral Impairment of *16p11.2del* mice after prenatal ERK pathway**
935 **inhibitor treatment.** WT or 16p11.2del -months old male or female mice treated with Veh or
936 Inh at E10.5 for 5 days. (a) Elevated plus maze shows a no change in percentage of time in open
937 arm, but decreased closed arm time in 16p11.2del mice that is rescued by inhibitor treatment
938 (* $p < 0.05$, # $p < 0.05$) (veh treated: nWT=25, nDel=22; inh treated: nWT=27, nDel=28); (b) Open
939 Field shows increased time spent in center in 16p11.2del mice that is rescued with inhibitor
940 treatment (** $p < 0.01$, # $p < 0.05$) (veh treated: nWT=23, nDel=20; inh treated: nWT=19, nDel=18).
941 (c) Fear conditioning shows increased freezing in 16p11.2del animals that improves with
942 inhibitor treatment (** $p < 0.01$) (veh treated: nWT=5, nDel=6; inh treated: nWT=11, nDel=11),
943 cond. stimulus: 85 dB sound at 2800 Hz for 30 sec.; unconditioned stimulus (US: 0.56mA).
944 Retention test performed 18 hrs later for 5 minutes in the absence of tone; (d) NOR was
945 evaluated in WT and 16p11.2del animals (# $p < 0.05$) (veh treated: nWT=16, nDel=12; inh treated:
946 nWT=8, nDel=16); (e) Naïve females were exposed to 3 WT pups placed in 3 corner of the cage,

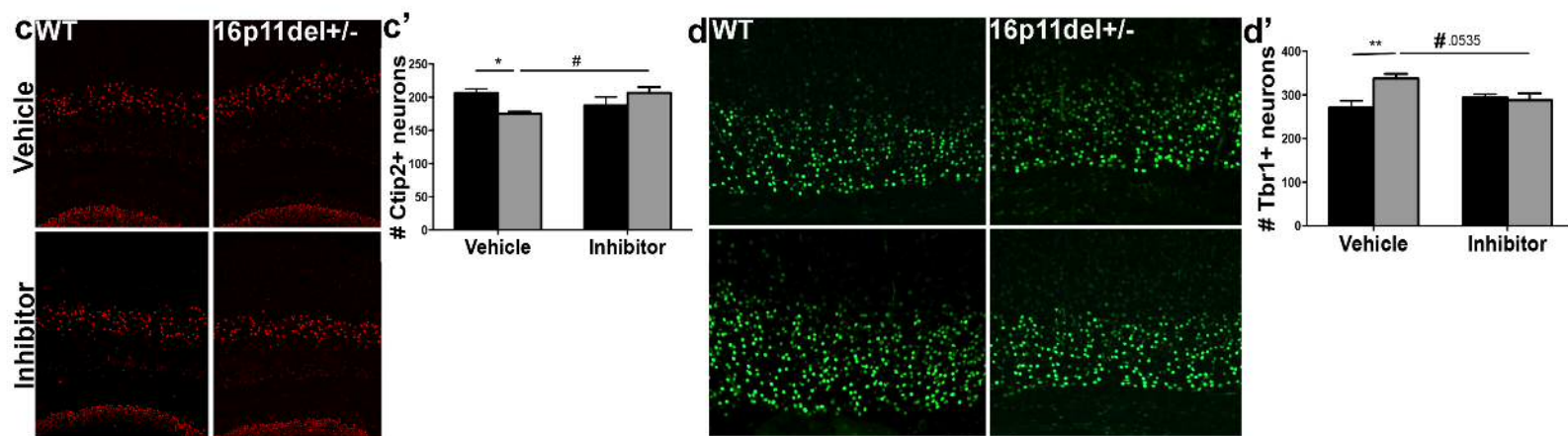
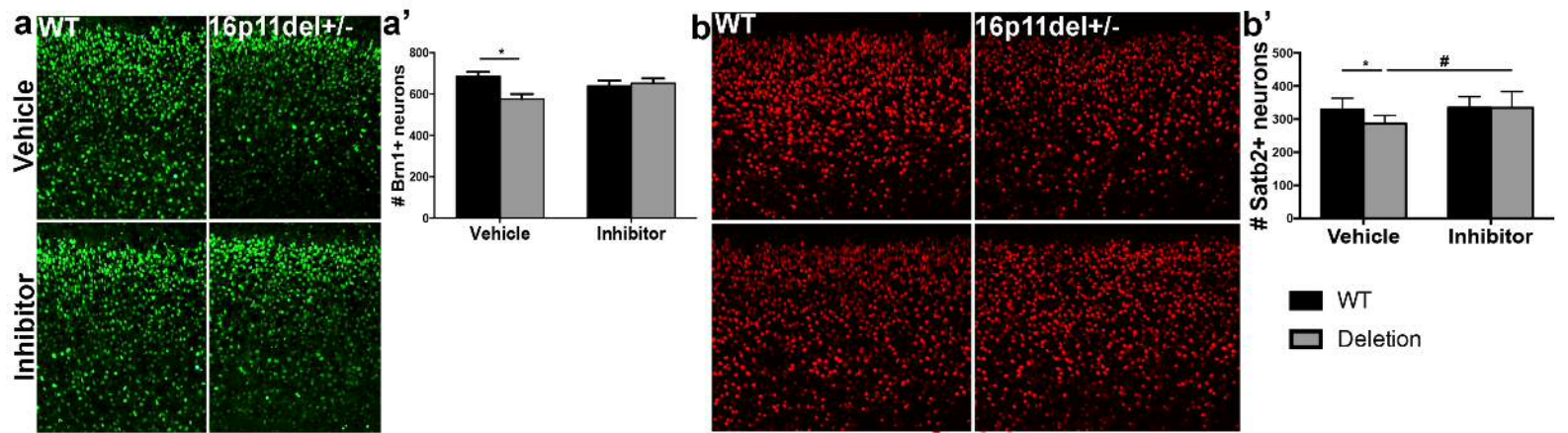
947 time to retrieve pups was recorded, (1st pup: **p<0.01; 2nd pup: **p<0.01; 3rd pup:
948 ***p=0.001) (veh treated: nWT=21, nDel=17; inh treated: nWT=6, nDel=6). (f) Mice were food
949 deprived for 24 hours, then placed in a cage containing one food pellet (teddy graham) buried
950 under normal cage bedding, time to retrieve was recorded (**p<0.01, #####p<0.0001) (veh
951 treated: nWT=22, nDel=22; inh treated: nWT=22, nDel=7). P values are from Bonferroni post-
952 hoc analysis (* compares WT to deletion, # compares vehicle deletion to inhibitor deletion).

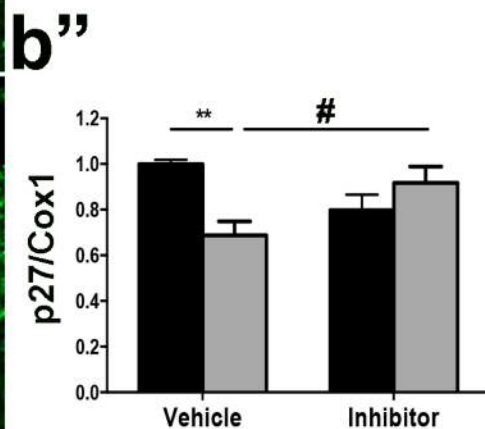
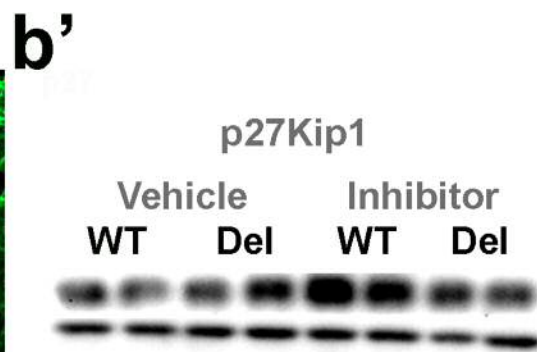
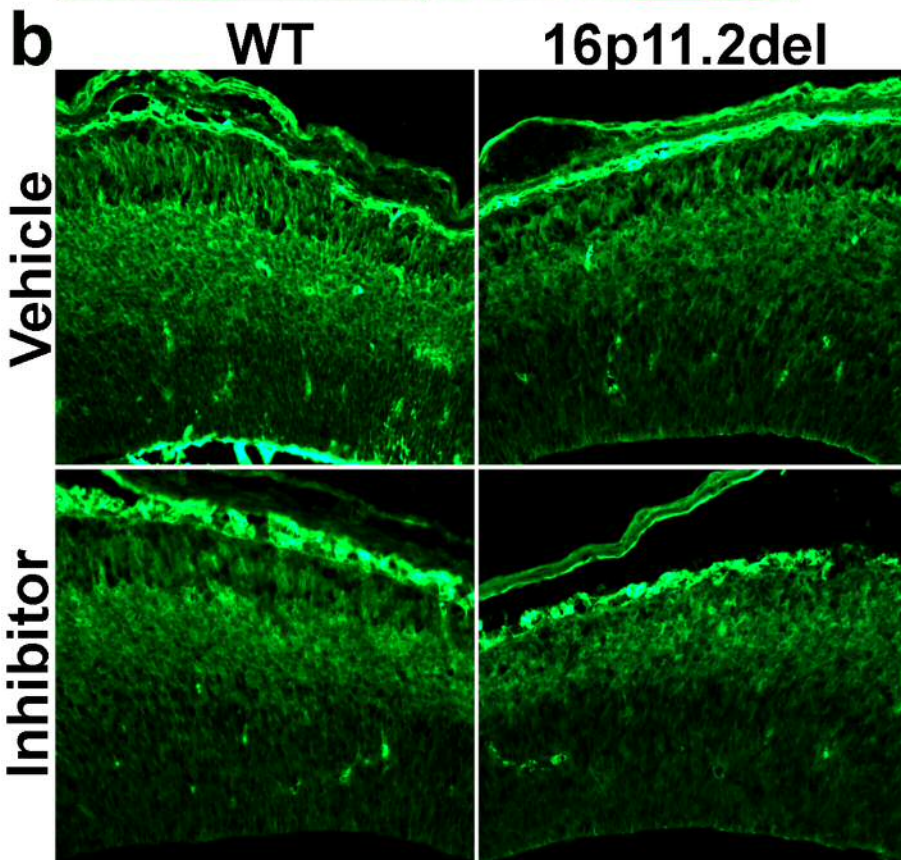
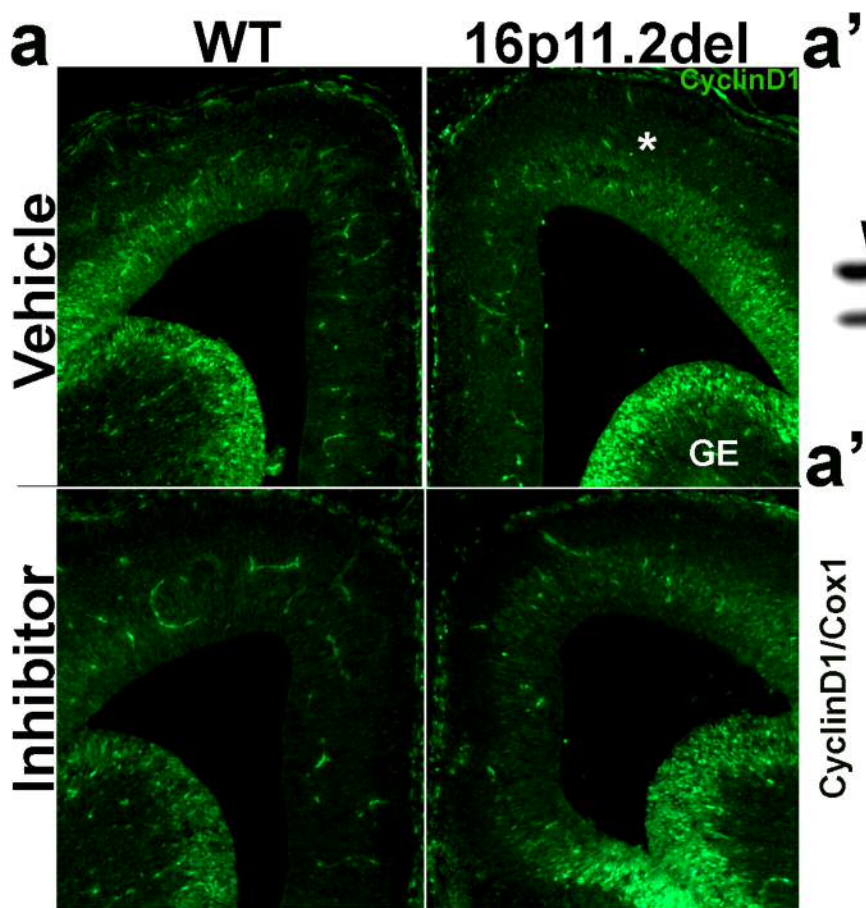
953

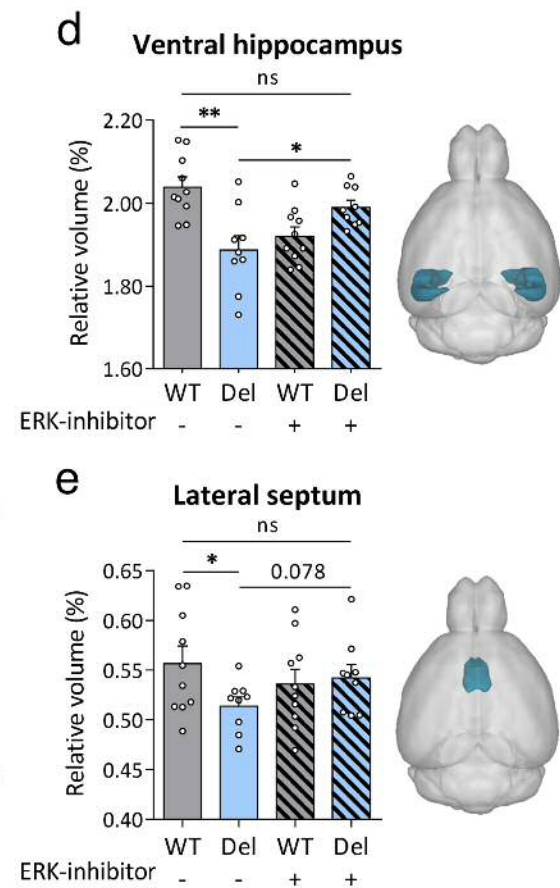
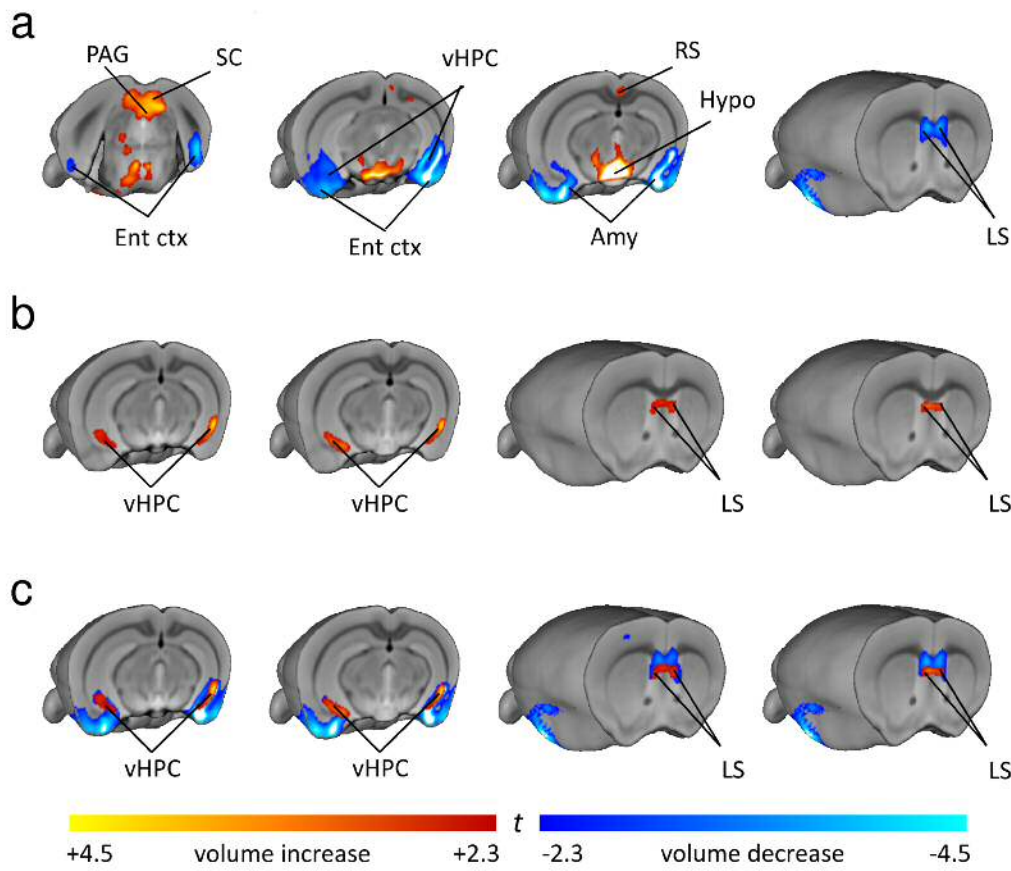
954 **Fig. 7 Postnatal treatment with ERK pathway inhibitor partially restores behavioral**
955 **deficits in adult *16p11.2del* mice.** WT or *16p11.2del* 3-months old male or female mice treated
956 with Veh or Inh at P90 for 5 days. (a) Elevated plus maze analysis of percentage of time in open
957 arm (*p<0.05), entries in open arm, immobility time (##p<0.01) and total distance traveled (veh
958 treated: nWT=15, nDel=11; inh treated: nWT=12, nDel=7); (b) Open Field analysis of entries
959 into center (##p<0.01), time spent in center and total distance traveled (veh treated: nWT=22,
960 nDel=17; inh treated: nWT=23, nDel=9). (c) ELISA performed on whole brain lysate of P90
961 mice (** p<0.05; #p<0.05) (veh treated: nWT=10, nDel=8; inh treated: nWT=7, nDel=5). (d)
962 Mice were food deprived for 24 hours, then placed in a cage containing one food pellet (teddy
963 graham) buried under normal cage bedding, time to retrieve (latency) was analyzed. P values are
964 from Bonferroni post-hoc analysis (* compares WT to deletion, # compares vehicle deletion to
965 inhibitor deletion).

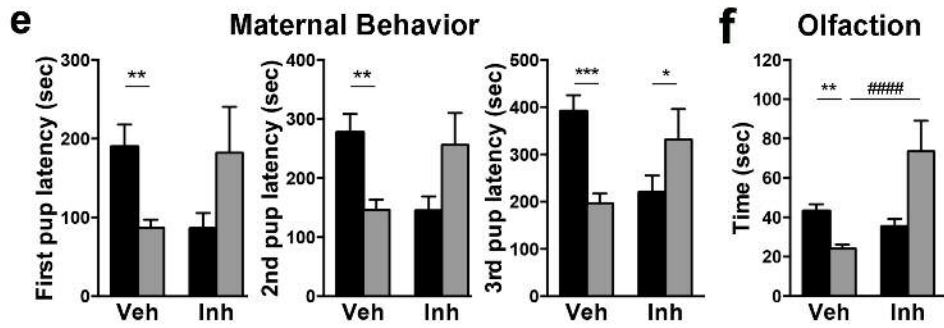
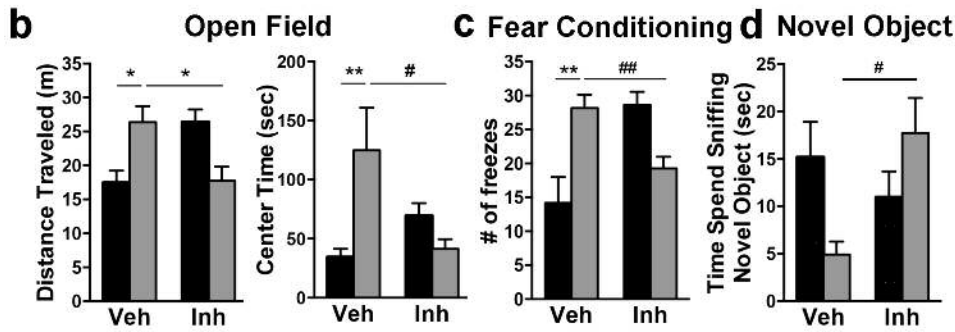
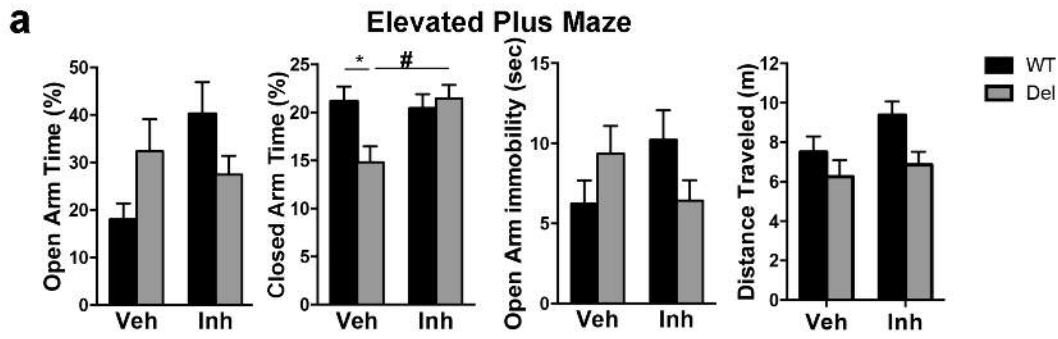


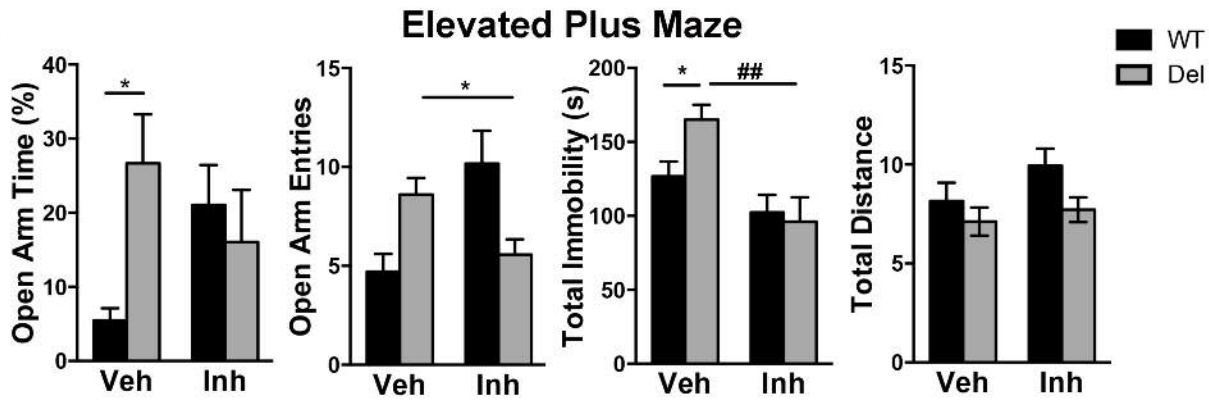
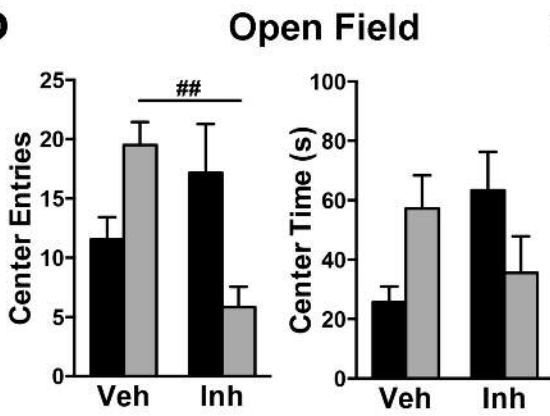
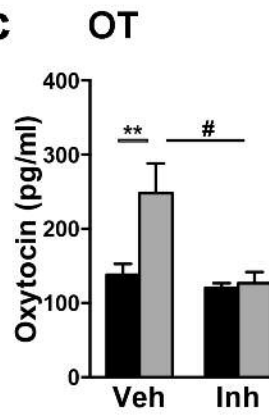










a**b****c****d**